THE JOURNAL OF BIOLOGICAL CHEMISTRY VOL. 291, NO. 46, pp. 24105–24120, November 11, 2016

Hyaluronan Production Regulates Metabolic and Cancer Stem-like Properties of Breast Cancer Cells via Hexosamine Biosynthetic Pathway-coupled HIF-1 Signaling*

Received for publication, August 5, 2016, and in revised form, September 23, 2016 Published, JBC Papers in Press, October 6, 2016, DOI 10.1074/jbc.M116.751263

Theerawut Chanmee[‡], Pawared Ontong[§], Tomomi Izumikawa[‡], Miho Higashide[‡], Nobutoshi Mochizuki[‡], Chatchadawalai Chokchaitaweesuk[‡], Manatsanan Khansai[‡¶], Kazuki Nakajima[‖], Ikuko Kakizaki[**], Prachya Kongtawelert[¶], Naoyuki Taniguchi[‡‡], and Naoki Itano[‡§1]

From the [‡]Department of Molecular Biosciences, Faculty of Life Sciences, and the [§]Division of Engineering (Biotechnology), Graduate School of Engineering, Kyoto Sangyo University, Kita-ku, Kyoto 603-8555, Japan, the [¶]Thailand Excellence Center for Tissue Engineering and Stem Cells, Department of Biochemistry, Faculty of Medicine, Chiang Mai University, Chiang Mai 50200, Thailand, the [‖]Division of Clinical Research Promotion and Support Center for Research Promotion, Fujita Health University School, Toyoake 470-1192, Japan, the [**]Department of Glycotechnology, Center for Advanced Medical Research, Hirosaki University Graduate School of Medicine, 5 Zaifu-cho, Hirosaki 036-8562, Japan, and the [‡‡]Disease Glycomics Team, Systems Glycobiology Research Group, Global Research Cluster, RIKEN-Max Planck Joint Research Center, RIKEN, Wako, Saitama 351-0198, Japan

Edited by Amanda Fosang

Cancer stem cells (CSCs) represent a small subpopulation of self-renewing oncogenic cells. As in many other stem cells, metabolic reprogramming has been implicated to be a key characteristic of CSCs. However, little is known about how the metabolic features of cancer cells are controlled to orchestrate their CSC-like properties. We recently demonstrated that hyaluronan (HA) overproduction allowed plastic cancer cells to revert to stem cell states. Here, we adopted stable isotope-assisted tracing and mass spectrometry profiling to elucidate the metabolic features of HA-overproducing breast cancer cells. These integrated approaches disclosed an acceleration of metabolic flux in the hexosamine biosynthetic pathway (HBP). A metabolic shift toward glycolysis was also evident by quantitative targeted metabolomics, which was validated by the expression profiles of key glycolytic enzymes. Forced expression of glutamine:fructose-6-phosphate amidotransferase 1 (GFAT1), an HBP rate-limiting enzyme, resembled the results of HA overproduction with regard to HIF-1α accumulation and glycolytic program, whereas GFAT1 inhibition significantly decreased HIF-1α protein level in HA-overproducing cancer cells. Moreover, inhibition of the HBP-HIF-1 axis abrogated HA-driven glycolytic enhancement and reduced the CSC-like subpopulation. Taken together, our results provide compelling evidence that HA production regulates the metabolic and CSC-like properties of breast cancer cells via HBP-coupled HIF-1 signaling.

In cancer cells, a high rate of glycolysis with increased lactate production in the presence of oxygen represents a metabolic switch from oxidative phosphorylation to aerobic glycolysis. This phenomenon, well known as the Warburg effect, is now considered to be a fundamental cellular response that affords tumor cells a key survival advantage (1, 2). The aberrant metabolic behavior of cancer cells is driven by alterations in transcription and signal transduction pathways, up-regulation of rate-limiting enzymes involved in glycolysis, and mitochondrial dysfunction. Currently, intense efforts are being made to understand the link between metabolism and the maintenance of cancer cell stemness (3). Recent evidence has suggested that metabolic reprogramming toward aerobic glycolysis may be a specific signature reflecting the undifferentiated and self-renewing state of cancer cells (4). However, our knowledge of how the metabolic features of cancer stem cells (CSCs)[2] are controlled remains fragmented.

Hypoxia-inducible factors (HIFs), which are master transcription factors governing hypoxic adaptation, activate the transcription of genes involved in various steps of energy metabolism (5) and are involved in crucial aspects of cancer biology. HIF is a heterodimer consisting of α- and β-subunits. The former subunit undergoes rapid degradation by a ubiquitin-proteasome system under normoxic conditions (6). Paradoxically, some subsets of cancer cells exhibit high levels of the HIF-1α regardless of oxygen concentration (7). Aberrant cell signaling that activates HIF-1α translation may partly account

* This work was supported by JSPS KAKENHI Grant 26430125 (to N. I.) and Tokyo Biochemical Research Foundation postdoctoral fellowships for Asian researchers in Japan (to T. C.). The authors declare that they have no conflicts of interest with the contents of this article.

[1] To whom correspondence should be addressed: Dept. of Molecular Biosciences, Faculty of Life Sciences, Kyoto Sangyo University, Kita-ku, Kyoto, Japan. Tel.: 81-75-705-3064; Fax: 81-75-705-3064; E-mail: itanon@cc.kyoto-su.ac.jp.

[2] The abbreviations used are: CSC, cancer stem cell; ALDOA, aldolase A; ALDOC, aldolase C; CE, capillary electrophoresis; cTg, conditional transgenic; DHAP, dihydroxyacetone phosphate; DBA, dimethyl-bisphenol A; DON, 6-diazo-5-oxo-L-norleucine; F1,6BP, fructose 1,6-bisphosphate; F6P, fructose 6-phosphate; F2,6BP, fructose 2,6-bisphosphate; GFAT1, glutamine:fructose-6-phosphate amidotransferase 1; GlcN, glucosamine; GlcN6P, glucosamine 6-phosphate; G6P, glucose 6-phosphate; G3P, glyceraldehyde 3-phosphate; HA, hyaluronan; HBP, hexosamine biosynthetic pathway; HIF, hypoxia-inducible factor; ESI, electrospray ionization; LDHA, lactate dehydrogenase A; PGAM1, phosphoglycerate mutase 1; PFK1, phosphofructokinase 1; PDK, pyruvate dehydrogenase kinase; PFKFB, 6-phosphofructo-2-kinase/fructose-2,6-bisphosphatase; GlcNAc, *N*-acetylglucosamine; HexNAc, *N*-acetylhexosamine; 4-OHT, 4-hydroxytamoxifen; qRT-PCR, quantitative RT-PCR; MMTV, mouse mammary tumor virus; MT, migration time; mTOR, mechanistic target of rapamycin.

for HIF-1α accumulation uncoupling to oxygen-responsive signaling in malignant cells (8). Alternatively, protein *O*-GlcNAcylation has recently been demonstrated to block HIF-1α degradation in breast cancer cells by suppressing its hydroxylation (9).

The hexosamine biosynthetic pathway (HBP) is a glucose metabolic pathway that branches off from the main glycolytic pathway. The major end product of the HBP is uridine diphosphate-*N*-acetylglucosamine (UDP-GlcNAc), which is utilized as a donor substrate in protein *O*-GlcNAcylation and glycoconjugate biosynthesis. As a rate-limiting enzyme of the HBP, glutamine:fructose-6-phosphate amidotransferase 1 (GFAT1) catalyzes the conversion of fructose 6-phosphate (F6P) to glucosamine 6-phosphate (GlcN6P) and dynamically modulates the cellular concentration of UDP-GlcNAc. Several HBP-related genes, including *GFAT1*, are overexpressed in human cancers (10), and glucose metabolism through the HBP has been implicated in cell growth and survival.

Hyaluronan (HA) is a linear polysaccharide and major constituent of the extracellular microenvironment. The vast majority of previous studies have demonstrated a crucial function of HA in tumorigenesis and tumor progression as a microenvironmental cue (11), and we recently provided evidence that excess HA production was a key element in the acquisition of CSC status (12). HA biosynthesis is regulated by three HA synthases (Has1–3) that serve to link UDP-GlcNAc and UDP-glucuronic acid substrates together in alternating β-1,3 and β-1,4 linkages. Considering that excess synthesis of this huge polysaccharide in cancer cells consumes large quantities of HA substrates, it becomes important to understand whether HA overproduction alters major metabolic pathways in cancer cells.

Here, we adopted an MS-based metabolomic approach for a comprehensive evaluation of major metabolites in HA-overproducing cancer cells. Metabolomic profiling and targeted analysis revealed that excessive HA production markedly shifted metabolic programs toward acceleration of HBP flux and glycolysis in breast cancer cells. Pharmacological and gene silencing studies suggested that HA-driven glycolytic enhancement was regulated by HIF-1 under the control of HBP flux. Moreover, abrogation of the HBP-HIF-1 axis suppressed the $CD44^{high}/CD24^{low}$ CSC-like subpopulation and mammosphere formation in HA-overproducing breast cancer cells. Collectively, we propose a novel mechanism by which HA production promotes a metabolic shift associated with CSC-like features in cancer cells via HBP-coupled HIF-1 signaling.

Results

HA Overproduction Accelerates Metabolic Flux in HBP—Our previous study demonstrated that HA overproduction allowed plastic cancer cell populations to revert to stem cell states partly via intracellular events. Because elevated HA biosynthesis in cancer cells may consume large quantities of UDP-sugar precursors, we hypothesized that substrate consumption may drive CSC-like properties through alterations in metabolic programs. A set of Has2-overexpressing breast cancer cells was compared with control counterparts to evaluate the influence of HA biosynthesis on metabolic programs (see "Experimental Procedures," Fig. 1, and Table 1). To measure the metabolic flux of UDP-sugar precursors in HA-overproducing cancer cells, we adopted stable isotope-assisted tracing methods using LC-MS. Has2-overexpressing $Has2^{\Delta Neo}$ and Has2 #4 breast cancer cells were metabolically labeled with $[^{13}C_6]$glucose, and the time-dependent changes in mass isotopomers of ^{13}C-labeled nucleotide sugars were compared with those of control counterparts ($Has2^{+Neo}$ and mock cells, respectively). Because prolonged labeling with $[^{13}C_6]$glucose might result in a complex labeling pattern, including partially labeled hexose and ribose, we limited the labeling period to 6 h. The separation of UDP-GlcNAc from UDP-GalNAc was incomplete under the HPLC conditions; therefore, the relative contribution of the UDP-GlcNAc synthetic pathway was assessed using the replacement ratios of each motif in $[^{13}C]$UDP-*N*-acetylhexosamine (UDP-HexNAc) as described previously (13). An unlabeled $[M-H]^-$ ion of UDP-HexNAc was detected at *m/z* 606.1 (Fig. 2*A*, 0 h). After labeling for 0.5 h, isotopic ions corresponding to 6- and 8-mass unit increases appeared at *m/z* 612.1 ($[^{13}C_6]$hexose residue) and *m/z* 614.1 ($[^{13}C_6]$hexose and $[^{13}C_2]$acetyl residues), respectively, in mock cells, indicating that UDP-HexNAc had been labeled with hexose and acetyl residues (Fig. 2*A*, 0.5 h). In contrast, $[^{13}C_5]$ribose-labeled ions had already appeared at *m/z* 617.1 ($[^{13}C_6]$hexose and $[^{13}C_5]$ribose residues) and *m/z* 619.1 ($[^{13}C_6]$hexose, $[^{13}C_5]$ribose, and $[^{13}C_2]$acetyl residues) after labeling for 0.5 h in Has2 #4 cells (Fig. 2*A*, 0.5 h). At 0.5 h, the replacement ratios of $[^{13}C_6]$hexose, $[^{13}C_5]$ribose, and $[^{13}C_2]$acetyl motifs in mock cells were 6.6 $\pm$ 1.3, 6.2 $\pm$ 1.7, and 2.4 $\pm$ 0.6%, which were increased at 37.7 $\pm$ 3.3, 19.1 $\pm$ 1.3, and 29.0 $\pm$ 2.6%, respectively, in Has2 #4 cells (Fig. 2*B*). When we further investigated the metabolic flux of UDP-sugar precursors in Has2 #3 cells exhibiting a moderate level of HA production, the replacement ratios of UDP-HexNAc motifs at 0.5 h were 12.6 $\pm$ 3.0% ($[^{13}C_6]$hexose), 8.6 $\pm$ 2.4% ($[^{13}C_5]$ribose), and 7.4 $\pm$ 1.9% ($[^{13}C_2]$acetyl residue), suggesting a good correlation between HA production and HBP flux. Similarly, the replacement ratios of $[^{13}C_6]$hexose, $[^{13}C_5]$ribose, and $[^{13}C_2]$acetyl motifs in control $Has2^{+Neo}$ cells were 14.5 $\pm$ 4.4, 6.8 $\pm$ 4.8, and 15.7 $\pm$ 6.3%, respectively, and 26.0 $\pm$ 2.2, 17.3 $\pm$ 3.7, and 22.6 $\pm$ 3.6%, respectively, in Has2-overexpressing $Has2^{\Delta Neo}$ cells (Fig. 2*B*). Taken together, the increased incorporation of isotopic ions into each motif of UDP-HexNAc clearly demonstrated an acceleration of HBP flux in HA-overproducing cancer cells.

HA Production Metabolically Regulates Glycolysis in Breast Cancer Cells—Because the HBP shares its first step with glycolysis, the acceleration of biosynthetic flux may affect the glycolytic pathway as well. To assess this notion, we comprehensively analyzed the glycolytic metabolites in HA-overproducing cancer cells using a CE-MS-based metabolomic approach. For major metabolites, Has2-overexpressing $Has2^{\Delta Neo}$ and Has2 #4 breast cancer cells were compared with control counterparts ($Has2^{+Neo}$ and mock cells, respectively). Has2-deficient $Has2^{\Delta/\Delta}$ cells were also compared with control $Has2^{flox/flox}$ cells to further evaluate the influence of HA biosynthesis on glycolysis (Fig. 1 and Table 1).

Functional validation of metabolomic data provided definitive evidence of a metabolic switch toward glycolysis. Metabolite profiling revealed lower levels of glucose 6-phosphate (G6P)

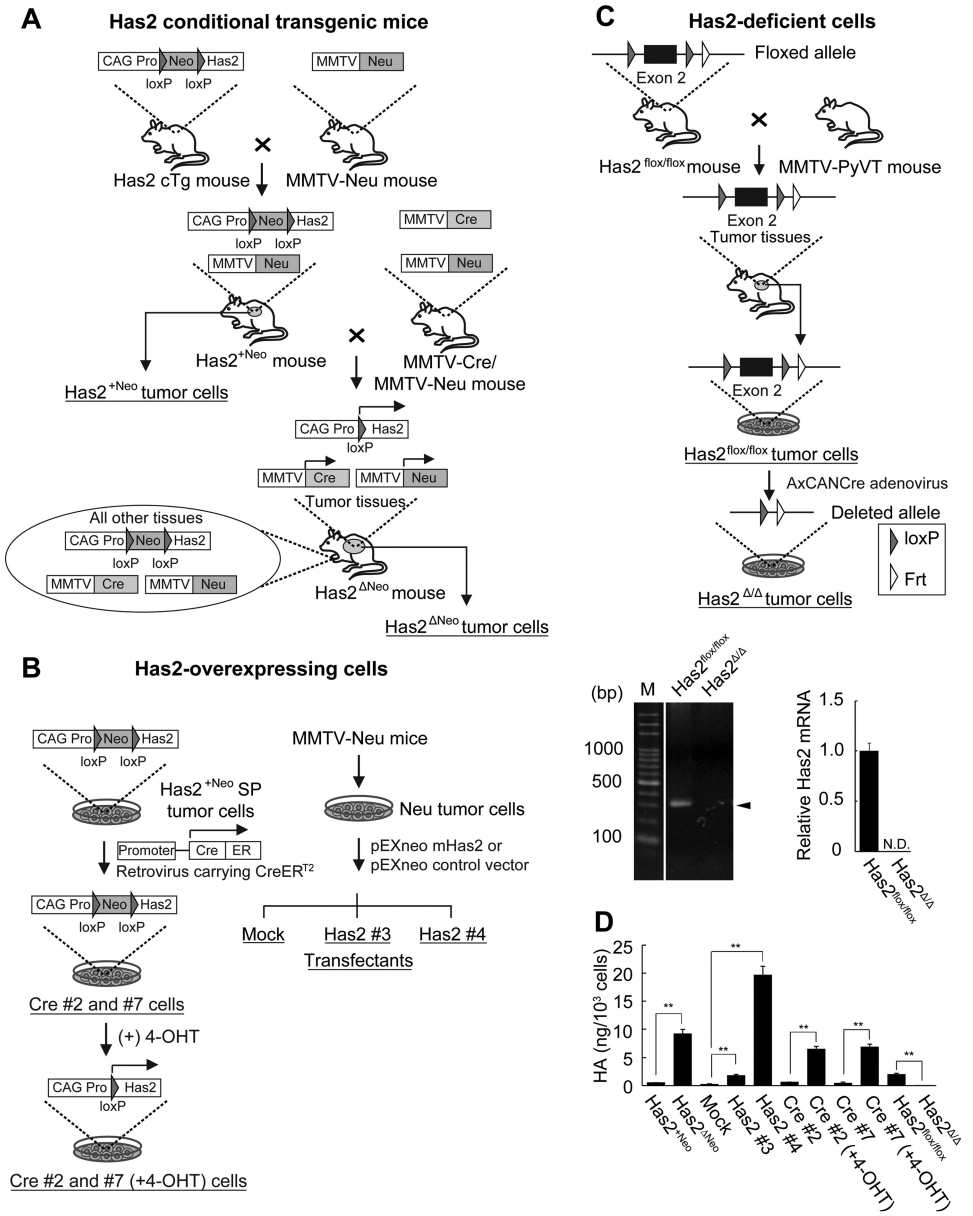

FIGURE 1. **Schematic representation of Has2-overexpressing and -deficient breast carcinoma cells.** *A*, establishment of Has2-overexpressing mammary tumor model mice. Has2 cTg mice were cross-bred with MMTV-Neu mammary tumor model mice to generate $Has2^{+Neo}$ mice. The $Has2^{+Neo}$ mice were further crossed with MMTV-Neu/MMTV-Cre double transgenic mice to generate $Has2^{\Delta Neo}$ mice. In $Has2^{\Delta Neo}$ mice expressing Cre recombinase under the control of the MMTV promoter, deletion of the Neo cassette and subsequent Has2 overexpression were achieved by Cre-mediated recombination of the transgene in spontaneous mammary tumors. In contrast, the expression of the *Has2* transgene was silent in control $Has2^{+Neo}$ mice due to a lack of Cre recombinase expression. $Has2^{\Delta Neo}$ and $Has2^{+Neo}$ tumor cells were established from primary mammary tumors of $Has2^{\Delta Neo}$ and $Has2^{+Neo}$ mice, respectively. *B*, establishment of Has2-overexpressing breast carcinoma cells. A side population (*SP*) of $Has2^{+Neo}$ tumor cells was infected with a retrovirus carrying $CreER^{T2}$ to obtain Cre #2 and #7 stable clones allowing inducible Has2 expression. In these clones, removal of the Neo cassette of the *Has2* transgene was achieved by $CreER^{T2}$-mediated recombination in response to 4-OHT. Stable cell lines (Has2 #3 and #4) constitutively expressing the *Has2* transgene were established from Neu tumor cells that were derived from primary mammary tumors developed in the MMTV-Neu mammary tumor model mice. *C*, targeted disruption of the mouse *Has2* gene in breast carcinoma cells. $Has2^{flox/flox}$ mice were back-crossed to MMTV-PyVT mice to generate mammary tumor model mice. $Has2^{flox/flox}$ tumor cells were established from primary mammary tumors of $Has2^{flox/flox}$ tumor model mice and infected with the AxCANCre adenovirus carrying the Cre recombinase to generate Has2-deficient $Has2^{\Delta/\Delta}$ cells. Exon 2 of the Has2 locus was flanked by two loxP sites in a floxed allele and was deleted by Cre-mediated recombination in a deleted allele. Genomic DNA isolated from $Has2^{flox/flox}$ and $Has2^{\Delta/\Delta}$ cells was subjected to genomic PCR analysis. As shown by the disappearance of the 307 bp band (*arrowhead*), exon 2 of the Has2 locus was effectively deleted in $Has2^{\Delta/\Delta}$ cells. In contrast, an intact floxed allele remained in $Has2^{flox/flox}$ cells. *M*, marker. Cre-mediated recombination of the Has2 locus induced an almost complete failure of Has2 expression in $Has2^{\Delta/\Delta}$ cells. *N.D.*, not detected. *D*, HA content in the conditioned medium was greatly increased for Has2-overexpressing $Has2^{\Delta Neo}$, Has2 #3, Has2 #4, Cre #2 (+4-OHT), and Cre #7 (+4-OHT) cells as compared with control $Has2^{+Neo}$, mock, Cre #2, and Cre #7 cells, respectively. Conversely, HA content was diminished in Has2-deficient $Has2^{\Delta/\Delta}$ cells. Data represent the mean ± S.D. (*error bars*) of three independent experiments. **, $p < 0.01$.

and F6P but a higher level of fructose 1,6-bisphosphate (F1,6BP) in Has2-overexpressing cancer cells than in control cells, indicating a higher conversion rate of F6P to F1,6BP (Fig. 3). F1,6BP level was slightly reduced in Has2-deficient $Has2^{\Delta/\Delta}$ cancer cells, although no significant changes in G6P or F6P levels were observed. In the Has2-overexpressing cells, meta-

TABLE 1

Characterization of Has2-overexpressing and -deficient tumor cells derived from mammary tumor models

Data represent the mean ± S. D. of three independent experiments. *, $p < 0.05$; **, $p < 0.01$ as compared with each control counterpart.

Tumor cell	Tumor model	$CD44^{high}/CD24^{low}$ subpopulation[a]	Mammosphere[b]	Doubling time[c]	Reference
$Has2^{+Neo}$	MMTV-Neu	0.8 ± 0.2	4.0 ± 1.0	28.0 ± 1.0	39
$Has2^{\Delta Neo}$	MMTV-Neu	29.4 ± 1.3**	34.7 ± 2.5**	29.2 ± 0.6	39
Mock	MMTV-Neu	0.8 ± 0.4	4.7 ± 1.5	24.0 ± 0.1	12
Has2 #3	MMTV-Neu	0.3 ± 0.1	4.3 ± 2.5	27.5 ± 0.5**	12
Has2 #4	MMTV-Neu	20.0 ± 3.3**	24.7 ± 2.5**	25.1 ± 0.1**	12
Cre #2	MMTV-Neu	12.3 ± 0.2	18.3 ± 3.5	29.1 ± 0.2	12
Cre #2 (+4-OHT)	MMTV-Neu	29.4 ± 0.1**	38.7 ± 3.5**	24.0 ± 0.1**	12
Cre #7	MMTV-Neu	4.6 ± 0.4	8.7 ± 1.5	27.3 ± 0.8	12
Cre #7 (+4-OHT)	MMTV-Neu	12.1 ± 0.5**	17.0 ± 2.0**	25.6 ± 0.2*	12
$Has2^{flox/flox}$	MMTV-PyVT	6.3 ± 0.4	9.3 ± 1.5	18.6 ± 0.2	
$Has2^{\Delta/\Delta}$	MMTV-PyVT	0.3 ± 0.1**	5.0 ± 1.0*	18.3 ± 0.2	

[a] Ratio of $CD44^{high}/CD24^{low}$ subpopulation (%).
[b] Number of mammospheres (spheres/5,000 cells).
[c] Doubling time (h) = $T \ln 2/\ln(Xe/Xb)$, where T is the incubation time in any units, Xb is the cell number at the beginning of the incubation time, and Xe is the cell number at the end of the incubation time.

bolic reprogramming was more apparent with the cleavage of F1,6BP into dihydroxyacetone phosphate (DHAP) and glyceraldehyde 3-phosphate (G3P) via fructose-bisphosphate aldolase (Fig. 3). Pyruvate and lactate generation, the most distinctive change associated with glycolysis, was significantly increased in Has2-overexpressing cancer cells, whereas a reduction in these metabolites was evident in Has2-deficient $Has2^{\Delta/\Delta}$ cancer cells (Fig. 3). Therefore, our metabolomic data implicated HA production in part of the machinery regulating energy metabolism.

Pathway-focused gene expression profiling with qRT-PCR demonstrated changes in the expression of glycolytic enzymes between Has2-overexpressing $Has2^{\Delta Neo}$ and control $Has2^{+Neo}$ cells. Among the genes involved in the enzymatic pathways of glucose and glycogen metabolism, those for three important glycolytic enzymes were markedly up-regulated in Has2-overexpressing cells. Specifically, $Has2^{\Delta Neo}$ cells exhibited a 3.5-fold increase in the transcription of aldolase C (ALDOC) over controls, and the gene expression of pyruvate dehydrogenase kinase, isozyme 1 (PDK1) and isozyme 2 (PDK2) was 16.3 and 5.0 times higher, respectively, than in control $Has2^{+Neo}$ cells (Table 2).

We subsequently carried out Western blotting analysis to analyze the expression of a panel of glycolytic enzymes. A set of Has2-overexpressing breast cancer cells was compared with control counterparts (Fig. 1 and Table 1). As determined by band intensity, Has2-overexpressing cells expressed a relatively higher level of 6-phosphofructo-2-kinase/fructose-2,6-bisphosphatase isoform 2 (PFKFB2) or isoform 3 (PFKFB3), which modulates cellular fructose 2,6-bisphosphate (F2,6BP) level (Fig. 4*A*). Because F2,6BP is a potent allosteric activator of phosphofructokinase 1 (PFK1), an enzyme catalyzing the conversion of F6P to F1,6BP and regulating the first rate-determining step of glycolysis, this finding provides a reasonable explanation for the high conversion rate of F6P to F1,6BP in Has2-overexpressing cells. Similarly, these cells expressed higher levels of lactate dehydrogenase A (LDHA) than did control counterparts (Fig. 4*A*). Standard biochemical measurements indicated that both LDH activity and lactate production were significantly elevated in Has2-overexpressing cancer cells but were decreased in Has2-deficient $Has2^{\Delta/\Delta}$ cancer cells (Fig. 4, *B* and *C*), which was consistent with metabolomic data and LDHA expression profiles. PDK1 protein expression was also increased in Has2-overexpressing cells in accordance with its gene expression profile (Fig. 4*A* and Table 2), indicating blockage of TCA cycle engagement via the inhibition of pyruvate dehydrogenase. In contrast, there were no changes in the expression of aldolase A (ALDOA), enolase-1, enolase-2, or phosphoglycerate mutase 1 (PGAM1) (Fig. 4*A*). These data confirmed the importance of HA production in the regulation of the critical steps of glucose metabolism switching.

HIF-1 Regulates Glycolytic Program in HA-overproducing Cancer Cells—As a master regulator of oxygen homeostasis, HIF-1 has been reported to directly associate with the gene expression of key glycolytic enzymes, such as PFKFB2/3, ALDOC, PDK1, and LDHA (14, 15). Because our metabolomic and gene expression analyses strongly suggested the activation of HIF-1 signaling in HA-overproducing cancer cells, we next investigated the mRNA and protein levels of HIF-1α. The HIF-1α protein level remained low in control $Has2^{+Neo}$ cells under normoxia (Fig. 5*A*) and clearly responded to hypoxia (Fig. 5*B*). When Has2-overexpressing breast cancer cells were compared with their respective control counterparts, the HIF-1α protein level was elevated in Has2-overexpressing cancer cells, even under normoxia. In contrast, a reduction in the HIF-1α protein level was evident in Has2-deficient $Has2^{\Delta/\Delta}$ cancer cells (Fig. 5*A*). No significant differences in the transcription level of HIF-1α were found (Fig. 5*A*).

To validate whether HIF-1 signaling controlled the up-regulation of glycolytic enzymes, we examined the expression of LDHA and PDK1 in Has2-overexpressing $Has2^{\Delta Neo}$ cells before and after exposure to echinomycin, an inhibitor of HIF-1 DNA binding activity. Pharmacological inhibition of HIF-1 using echinomycin moderately suppressed the expression of LDHA and PDK1 and exerted negative effects on LDH activity in Has2-overexpressing $Has2^{\Delta Neo}$ cells (Fig. 5*C*). These observations strongly indicated HIF-1 to be a critical mediator involved in the regulation of glycolytic metabolism. We next silenced HIF-1α gene expression in $Has2^{\Delta Neo}$ cells to further confirm whether HIF-1 was a critical mediator involved in the regulation of glycolytic metabolism. Two different shRNAs against murine HIF-1α mRNA were introduced into $Has2^{\Delta Neo}$ cells using a retroviral vector, and three stably transduced cell clones for each shRNA were established. As a negative control

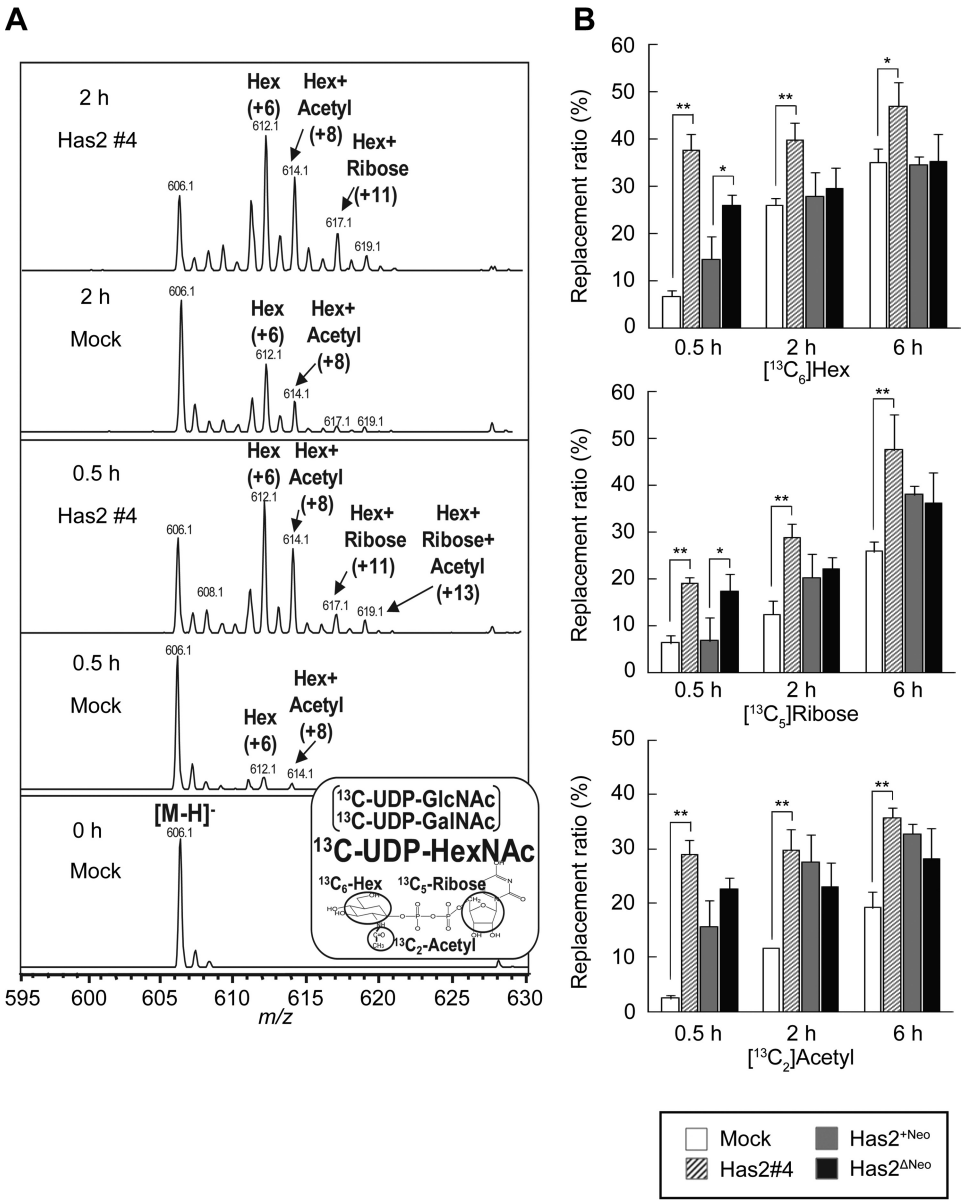

FIGURE 2. **LC-MS profiles of [^{13}C]UDP-HexNAc.** Has2-overexpressing (Has2 #4 and Has2$^{\Delta Neo}$) and control (mock and Has2^{+Neo}) cancer cells were cultured in medium containing 5.5 mM [$^{13}C_6$]glucose for 0, 0.5, 2, or 6 h, and time-dependent changes in mass isotopomers of ^{13}C-labeled UDP-HexNAc were monitored using an LC-MS system. *A*, mass isotopomers of [^{13}C]UDP-HexNAc. *B*, replacement ratios of [$^{13}C_6$]hexose (*Hex*), [$^{13}C_5$]ribose (*Hex* + *Ribose*), and [$^{13}C_2$]acetyl residue (*Hex* + *Acetyl*) motifs in UDP-HexNAc isotopomers. Mock (*open bars*), Has2 #4 (*striped bars*), Has2^{+Neo} (*gray bars*), and Has2$^{\Delta Neo}$ (*black bars*) cells were extracted at the indicated times and subjected to LC-MS analysis. Data represent the mean ± S.D. (*error bars*) of three independent experiments. *, $p < 0.05$; **, $p < 0.01$.

for the experiments, Has2$^{\Delta Neo}$ cells were infected with control retroviral shRNA encoding a scrambled sequence that would not lead to the specific degradation of any cellular message. The transduced cells were analyzed for levels of endogenous HIF-1α by Western blot analysis. HIF-1α knockdown decreased its expression by up to 90% as compared with Has2$^{\Delta Neo}$ cells with control shRNA (Fig. 5*D*). Consistent with the reduced expression of HIF-1α, the expression of LDHA and PDK1 was suppressed in these knockdown cells. LDH activity was significantly reduced in these knockdown cells as well (Fig. 5*D*).

Accelerated HBP Flux Activates Glycolysis through HIF-1 Signaling—To investigate the role of the HBP in HIF-1 signaling and the glycolytic pathway, we established several Has2^{+Neo} clones that expressed various levels of human GFAT1 and classified these clones into three groups according to expression level as low (GFAT #7, #8, and #11), moderate (GFAT #3 and #6), and high expressers (GFAT #4, #5, #9, and #10) (Fig. 6*A*). Transfectants with no GFAT1 expression were established as negative controls (GFAT #1 and #2). HPLC analysis of cellular UDP-sugars indicated an increased flow rate of UDP-HexNAc in accordance with GFAT1 expression (Fig. 6*B*). Intriguingly, forced GFAT1 expression significantly increased HIF-1α and LDHA protein levels in a dose-dependent manner (Fig. 6*A*). In agreement with LDHA expression, LDH activity and lactate production were also significantly increased in the GFAT1 expressers (Fig. 6, *C* and *D*). Together with the above results, these findings strongly implied that accelerated HBP flux acti-

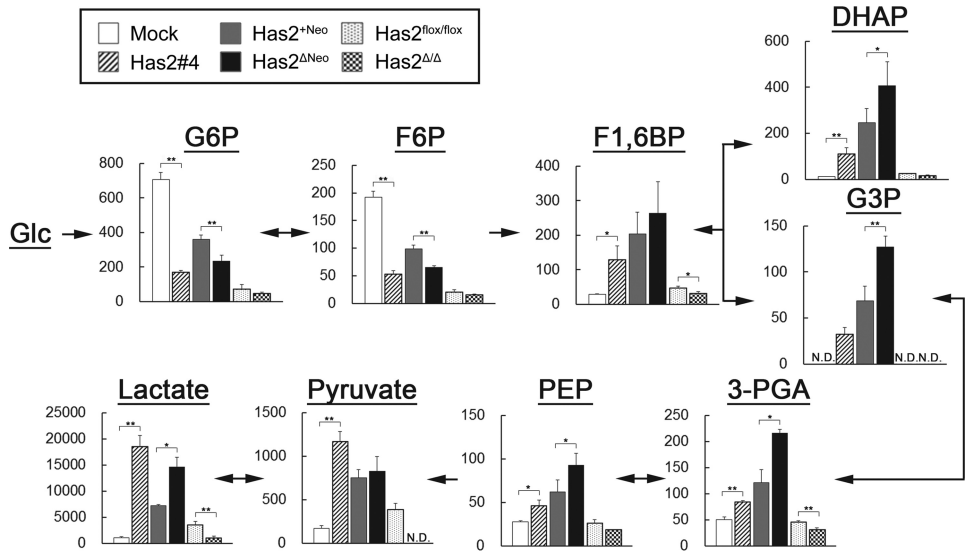

FIGURE 3. **Metabolomic analysis of glycolytic intermediates in Has2-overexpressing and -deficient breast cancer cells.** Has2-overexpressing and -deficient cancer cells were extracted and subjected to CE-MS analysis for G6P, F6P, F1,6BP, DHAP, G3P, 3-phosphoglycerate (*3-PGA*), phosphoenolpyruvate (*PEP*), pyruvate, and lactate. Mock (*open bars*), Has2 #4 (*striped bars*), Has2^{+Neo} (*gray bars*), Has2$^{\Delta Neo}$ (*black bars*), Has2$^{flox/flox}$ (*dotted bars*), and Has2$^{\Delta/\Delta}$ (*checkered bars*) cells are shown. Metabolite concentrations (pmol/10^6 cells) were superimposed on a glycolytic pathway map. *N.D.*, not detected. Data represent the mean ± S.D. (*error bars*) of three independent experiments. All *p* values were evaluated by the Wilcoxon matched pair test. *, $p < 0.05$; **, $p < 0.01$.

TABLE 2

Changes in expression for genes involved in the glucose metabolism between Has2^{+Neo} and Has2$^{\Delta Neo}$ breast cancer cells

Genes that exhibit a ≥3-fold change in expression between Has2^{+Neo} and Has2$^{\Delta Neo}$ breast cancer cells are listed.

Symbol	GenBank™ (Refseq)	Gene name	-Fold change Has2$^{\Delta Neo}$/Has2^{+Neo}	Average $\Delta\Delta C_t$	
				Has2$^{\Delta Neo}$	Has2^{+Neo}
Aldoc	NM_009657	Aldolase C	3.51	8.99	7.18
Gys1	NM_030678	Glycogen synthase 1	0.33	3.90	5.48
Pdk1	NM_011044	Pyruvate dehydrogenase kinase, isoenzyme 1	16.27	10.05	6.03
Pdk2	NM_028994	Pyruvate dehydrogenase kinase, isoenzyme 2	4.97	12.58	10.27
Pgm1	NM_025700	Phosphoglucomutase 1	0.30	4.79	6.51
Suclg1	NM_019879	Succinate-CoA ligase, GDP-forming, α subunit	0.30	0.94	2.68

vated HIF-1 signaling and potentiated the glycolysis pathway by up-regulation of key enzymes.

To ascertain whether HA overproduction controlled the expression of glycolytic enzymes via HBP-coupled HIF-1 signaling, Has2$^{\Delta Neo}$ cells were treated with a competitive GFAT1 antagonist, 6-diazo-5-oxo-L-norleucine (DON). DON exposure dose-dependently decreased HIF-1α protein levels (Fig. 7*A*) and concomitantly reduced the expression of the key glycolytic enzymes LDHA and PDK1 (Fig. 7*B*) along with LDH activity (Fig. 7*C*). DON is a glutamine analogue that has broader effects on other amidotransferases (16, 17). Glucosamine (GlcN) transported by the glucose transporter systems is phosphorylated by hexokinase to form GlcN6P and bypass the GFAT-mediated step of the HBP, resulting in a rapid production of UDP-GlcNAc. Thus, we performed a rescue experiment in which DON-treated Has2$^{\Delta Neo}$ cells were exposed to GlcN. Exogenous supplementation of GlcN in culture medium rescued the levels of HIF-1α and key glycolytic enzymes as well as LDH activity in DON-treated Has2$^{\Delta Neo}$ cells (Fig. 7, *B* and *C*). To further verify the role of HBP flux in the activation of HIF-1 signaling, we silenced *GFAT1* gene expression in Has2$^{\Delta Neo}$ cells using RNA interference. Two different shRNAs against murine GFAT1 mRNA were introduced into Has2$^{\Delta Neo}$ cells using a lentiviral vector. As a negative control for the experiments, Has2$^{\Delta Neo}$ cells were infected with control lentiviral shRNA encoding a scrambled sequence that would not lead to the specific degradation of any cellular message. The transduced cells were analyzed for levels of endogenous GFAT1 mRNA by qRT-PCR and for levels of endogenous HIF-1α by Western blotting analysis. GFAT1 knockdown decreased its expression by ~70% as compared with Has2$^{\Delta Neo}$ cells with control shRNA (Fig. 7*D*). GFAT1 knockdown significantly reduced HIF-1α protein levels in Has2-overexpressing cancer cells, suggesting a role of the HBP in HIF-1 accumulation (Fig. 7*D*). Consistent with the reduced expression of HIF-1α, the expression of LDHA and PDK1 was suppressed in these knockdown cells. LDH activity was significantly reduced in these knockdown cells as well (Fig. 7*D*).

Feedback Regulation of HA Production by HBP-coupled HIF-1 Signaling—The above observation that HA production regulated HBP-coupled HIF-1 signaling prompted us to investigate the feedback regulation of HA production. We silenced *HIF-1α* gene expression in Has2$^{\Delta Neo}$ cells to examine whether HIF-1 participated in the regulation of HA production. Indeed, HIF-1α knockdown moderately decreased HA production as compared with Has2$^{\Delta Neo}$ cells with control shRNA (Fig. 8*A*). To assess whether acceleration of HBP flux stimulated HA production, we compared HA production among Has2^{+Neo}

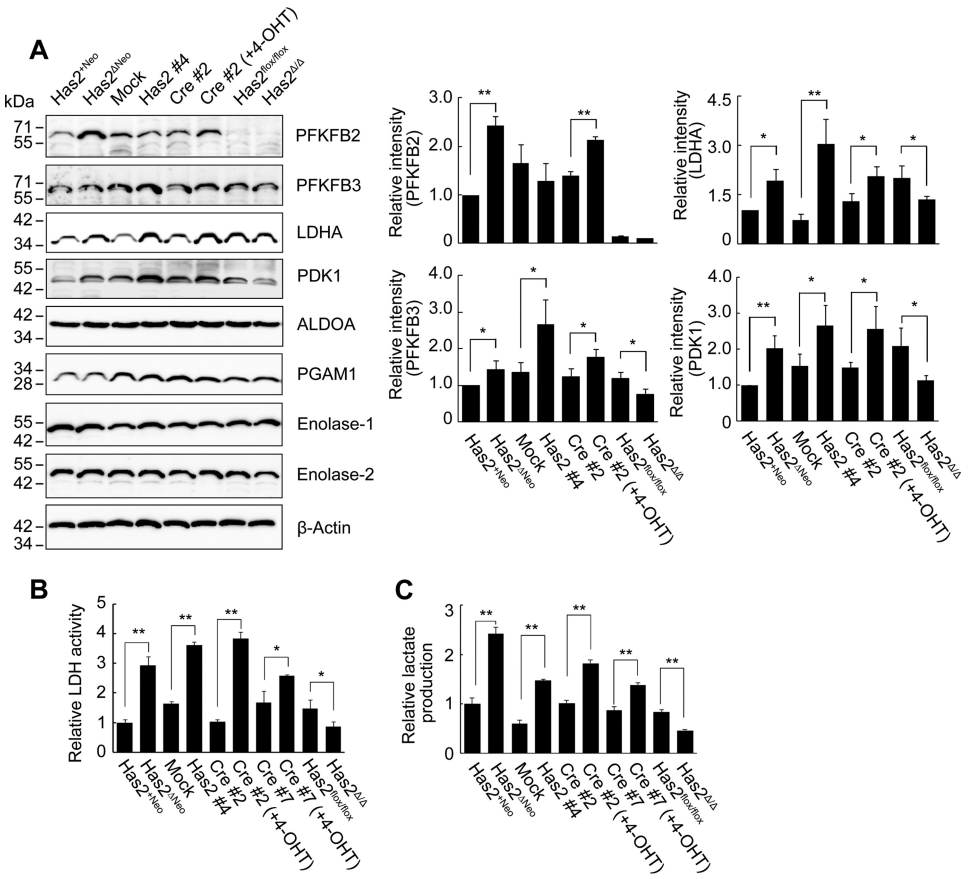

FIGURE 4. **Expression of glycolysis-related proteins in Has2-overexpressing and -deficient cells.** *A*, Western blot analysis for the expression of PFKFB2, PFKFB3, LDHA, PDK1, ALDOA, PGAM1, enolase-1, and enolase-2. Has2-overexpressing $Has2^{\Delta Neo}$, Has2 #4, and Cre #2 (+4-OHT) cells were compared with control $Has2^{+Neo}$, mock, and Cre #2 cells, respectively. Has2-deficient $Has2^{\Delta/\Delta}$ cells were also compared with control $Has2^{flox/flox}$ cells. *β*-Actin was used as an internal control. Band intensities were quantified by densitometric analysis using ImageJ software. Data represent the mean ± S.D. (*error bars*) of three independent experiments. *, $p < 0.05$; **, $p < 0.01$ as compared with each control counterpart. *B* and *C*, LDH activity and lactate production in Has2-overexpressing and -deficient cells. Cell lysates and conditioned medium were measured for LDH activity (*B*) and lactate production (*C*), respectively. Data represent the mean ± S.D. of three independent experiments. *, $p < 0.05$; **, $p < 0.01$ as compared with each control counterpart.

clones with various expression levels of GFAT1. HA production was dose-dependently increased in concert with the expression of GFAT1 (Fig. 8*B*). Conversely, GFAT1 knockdown decreased HA production by ~70% as compared with $Has2^{\Delta Neo}$ cells with control shRNA (Fig. 8*C*). These data suggested the existence of a positive feedback loop generated by HBP/HIF-1 and HA production.

HBP-coupled HIF-1 Signaling Controls CSC-like Properties—As summarized in Table 1, Has2-overexpressing cancer cells contained relatively higher proportions of CSC-like cells, whereas Has2-deficient cancer cells reduced the CSC-like subpopulations. These observations led us to explore the possibility that HA production may influence the CSC signatures via HBP-coupled HIF-1 signaling. To this end, $Has2^{\Delta Neo}$ cells were treated with the HIF inhibitor dimethyl-bisphenol A (DBA) for 7 days and assessed for the expression of CD44 and CD24 by flow cytometric analysis. DBA significantly reduced the $CD44^{high}/CD24^{low}$ CSC-like subpopulation in a dose-dependent manner (Fig. 9*A*). Comparable findings were observed for another HIF inhibitor, echinomycin (Fig. 9*A*). Consistent with the results of pharmacological inhibition, knockdown of HIF-1α in $Has2^{\Delta Neo}$ cells markedly reduced the $CD44^{high}/CD24^{low}$ CSC-like subpopulation (Fig. 9*A*). CSCs have been reported to form floating spherical colonies termed mammospheres to survive and proliferate in anchorage-independent conditions (18). The pharmacological inhibition or gene silencing significantly inhibited mammosphere formation in $Has2^{\Delta Neo}$ cells (Fig. 9*B*), which suggested an important role of HIF-1 signaling in maintaining CSC-like properties. To verify whether HBP inhibition affected CSC-like properties, $Has2^{\Delta Neo}$ cells were treated with the GFAT inhibitor DON for 7 days. As evidenced by flow cytometric analysis, this pharmacological inhibition reduced the $CD44^{high}/CD24^{low}$ subpopulation in $Has2^{\Delta Neo}$ cells (Fig. 9*A*). DON treatment also diminished the number of mammospheres in $Has2^{\Delta Neo}$ cells (Fig. 9*B*). *GFAT1* gene expression was then silenced in $Has2^{\Delta Neo}$ cells using a lentiviral vector, and knockdown cells were analyzed for the expression of CD44 and CD24 by flow cytometric analysis. GFP-positive cells carrying a gene-silencing vector, but not GFP-negative cells, clearly had a reduced $CD44^{high}/CD24^{low}$ subpopulation (Fig. 9*C*). No significant change in this subpopulation was observed in GFP-positive cells carrying a control vector (Fig. 9*C*). Taken together, our results indicated that HA production drove CSC-like properties via HBP-coupled HIF-1α signaling.

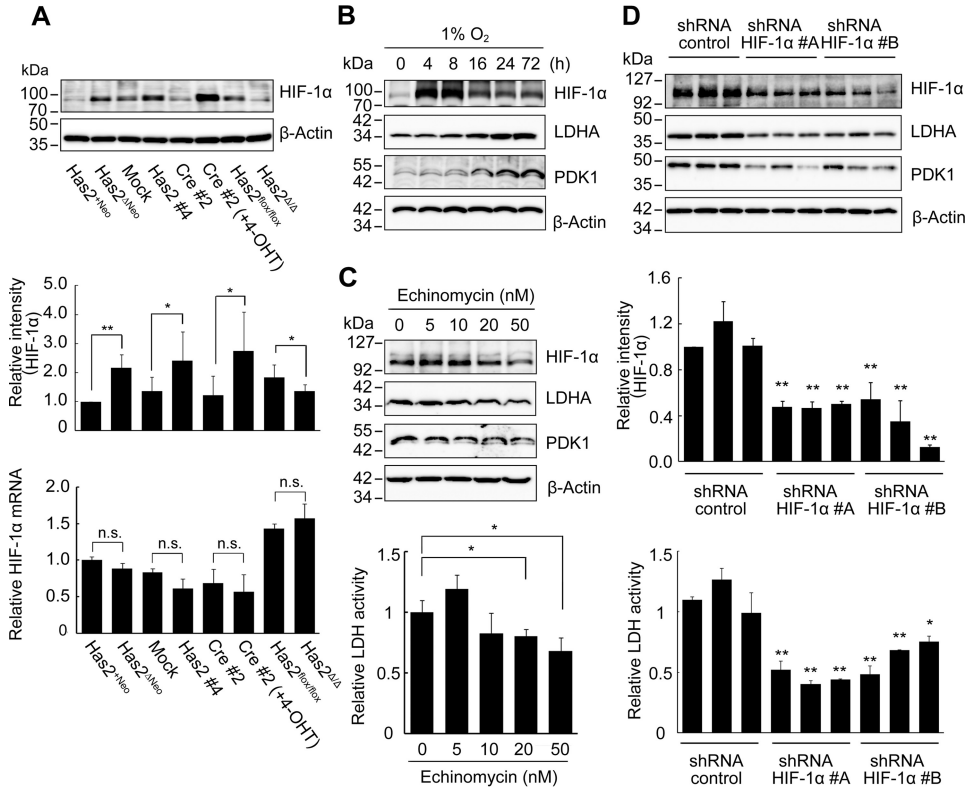

FIGURE 5. **HA production regulates glycolysis via HIF-1.** *A*, HIF-1α expression in Has2-overexpressing and -deficient breast cancer cells. Western blot analysis was conducted to determine the expression of HIF-1α in Has2-overexpressing and -deficient breast cancer cells. β-Actin was used as an internal control. Band intensities were quantified by densitometric analysis using ImageJ software. qRT-PCR was performed to evaluate HIF-1α mRNA expression. Data represent the mean $\pm$ S.D. (*error bars*) of three independent experiments. *, $p < 0.05$; **, $p < 0.01$ as compared with each control counterpart. *n.s.*, not significant. *B*, expression of HIF-1α and glycolytic enzymes under hypoxic conditions. $Has2^{+Neo}$ cells were exposed to 1% O_2 for to 72 h. Cell lysates were prepared and subjected to Western blotting analysis for the expression of HIF-1α, LDHA, and PDK1. β-Actin was used as an internal control. *C*, suppression of glycolysis by HIF-1α inhibition. $Has2^{\Delta Neo}$ cells were treated with various doses of echinomycin for 72 h. Cell lysates were prepared and subjected to Western blotting analysis for the expression of HIF-1α, LDHA, and PDK1. β-Actin was used as an internal control. LDH activity 72 h after echinomycin treatment was measured as described under "Experimental Procedures." Data represent the mean $\pm$ S.D. of three independent experiments. *, $p < 0.05$ as compared with untreated cells. *D*, effects of HIF-1α knockdown on glycolysis in Has2-overexpressing cancer cells. $Has2^{\Delta Neo}$ cells were infected with lentiviruses carrying two different HIF-1α shRNAs (#*A* and #*B*) or a control shRNA. Three stable clones for each shRNA were isolated and then subjected to Western blot analysis for the expression of HIF-1α, LDHA, and PDK1. β-Actin was used as an internal control. Band intensities were quantified by densitometric analysis using ImageJ software. Data represent the mean $\pm$ S.D. of three independent experiments. **, $p < 0.01$ as compared with the control shRNA cells. HIF-1α knockdown cells were measured for LDH activity. Data represent the mean $\pm$ S.D. of three independent experiments. *, $p < 0.05$; **, $p < 0.01$ as compared with the control shRNA cells.

Discussion

The present study adopted stable isotope-assisted tracing and metabolomic approaches to comprehensively monitor the metabolic changes associated with HA production and demonstrated that HA-overproducing cancer cells accelerated HBP flux and shifted cellular metabolism toward glycolysis. Our findings further point to a novel mechanism by which HA production regulates metabolic and CSC-like properties in cancer cells via HBP-coupled HIF-1 signaling (Fig. 10).

Excess HA synthesis in cancer cells consumes large quantities of substrates and accordingly diminishes the UDP-sugar pool. These cells may sense such UDP-sugar depletion and subsequently accelerate their biosynthetic flux by compensatory mechanisms maintaining energy homeostasis. The HBP branches off from the main glycolytic pathway and functions as a cellular nutrient sensor to maintain sufficient levels of UDP-sugars. The activation of PI3K-Akt pathway stimulates glucose uptake by promoting increased glucose metabolism (19), thus supplying more UDP-GlcNAc. c-Myc also increases glucose flux from the main glycolytic pathway to the HBP (20). Given the fact that both PI3K/Akt signaling and c-Myc expression represent downstream targets of HA signaling (11, 21), it will also be imperative to clarify the regulatory mechanisms of the feedback loop between HA production and glucose metabolism.

The current data suggested the existence of a positive feedback loop generated by HBP/HIF-1 and HA production. The acceleration of HBP flux elevates cellular UDP-GlcNAc and drives protein *O*-GlcNAcylation. The stability of Has2 has been shown to be dynamically regulated by *O*-GlcNAcylation. A loss of *O*-GlcNAc at a serine residue leads to rapid Has2 degradation in proteasomes (22). It is therefore plausible that *O*-GlcNAcylation of this enzyme may be a critical checkpoint for regulating the positive feedback loop. The HIF-1 signaling pathway regulates the rate of glucose uptake by glucose transporters. A possible mechanism for our proposed positive feedback loop is therefore that activation of HIF-1 signaling accelerates glucose entry, which subsequently increases the supply of UDP-sugar precursors for HA biosynthesis.

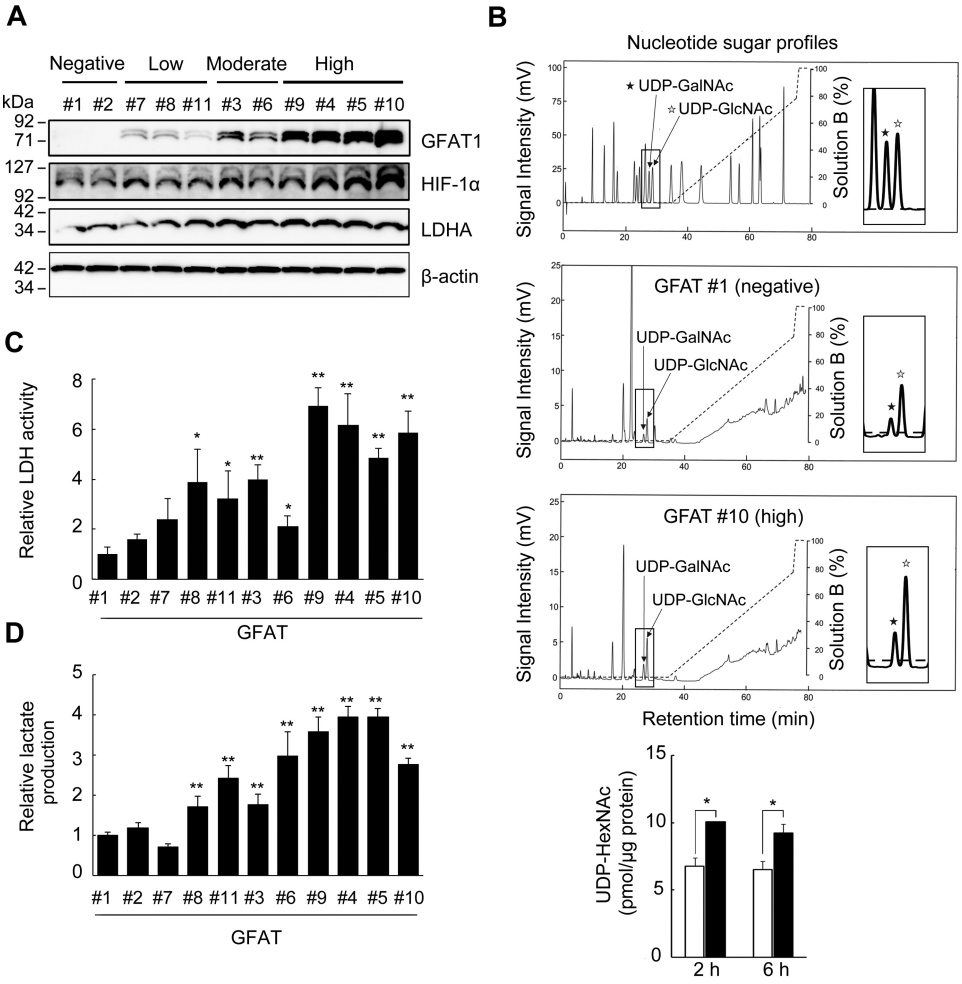

FIGURE 6. **Forced GFAT1 expression potentiates HIF-1α expression and lactate production.** *A*, Western blot analysis for the expression of GFAT1, HIF-1α, and LDHA in GFAT1 transfectants. Has2^{+Neo} cells were transfected with expression plasmids carrying human GFAT1 to establish stable transfectants expressing various levels of GFAT1. Cell lysates from the GFAT1 transfectants were subjected to Western blotting analysis. β-Actin was used as an internal control. *B*, production of UDP-HexNAc by forced GFAT1 expression. GFAT #1 (negative) and #10 (high) cells were cultured for 24 h in glucose-free DMEM and then further incubated in normal culture medium for up to 6 h. UDP-HexNAc production was monitored using HPLC and compared between GFAT #1 (*open bars*) and #10 (*black bars*) cells. Data represent the mean ± S.D. (*error bars*) of three independent experiments. *, $p < 0.05$. *C*, LDH activity in the GFAT1 transfectants. Cell lysates from the GFAT1 transfectants were measured for LDH activity. Data represent the mean ± S.D. of three independent experiments. *, $p < 0.05$; **, $p < 0.01$ as compared with the GFAT #1 clone. *D*, lactate production in the GFAT1 transfectants. Conditioned media from the GFAT1 transfectants were measured for lactate production. Data represent the mean ± S.D. of three independent experiments. **, $p < 0.01$ as compared with the GFAT #1 clone.

HIF-1 is a key transcriptional regulator of genes involved in the hypoxic response of cancer cells whose high expression has been well correlated with a poor prognosis in various tumor types. HIF-1 may promote the survival, self-renewal, and tumorigenesis of CSCs under hypoxic conditions. A recent study demonstrated that hypoxia enhanced the self-renewal activity of CD133-positive glioma stem cells through activation of HIF-1α (23). In the current study, the fact that inhibition of HIF-1 signaling suppressed CSC-like cells implied its critical role in the regulation of CSC-like properties in HA-overproducing cancer cells.

Under normoxic conditions, hydroxylated HIF-1α undergoes degradation in a proteasome-dependent manner, although other reports have also shown that subsets of cancer cells exhibit high levels of HIF-1α regardless of the surrounding oxygen concentration (7). A part of this controversy can be explained by the fact that several growth factors and cytokines, such as insulin, interleukin-1, and tumor necrosis factor-α, enhance HIF-1α translation (24–26). Intracellularly, oncogenes and downstream PI3K/Akt/mTOR signaling also appear to be involved in the regulation of HIF-1 translation (7, 27). Furthermore, loss of either tumor suppressor protein PTEN or factor inhibiting HIF-1 leads to HIF-1α stabilization (28) and increases its transactivation function (29). In addition, reactive oxygen species production has been demonstrated as specifically required for HIF-1α stabilization (30, 31), and a novel mechanism involved in HBP flux has recently been proposed to regulate the stabilization of HIF-1α via changes in protein *O*-GlcNAcylation (9). Our findings indicate a strong significance of the HBP in HA-dependent HIF-1α accumulation, although the precise underlying mechanism requires further investigation.

CSCs reside in a special microenvironment or niche that provides the cues necessary for survival and propagation. The interactions between HA and its receptor, CD44, evoke a wide range of signals required for CSC stemness, such as those with

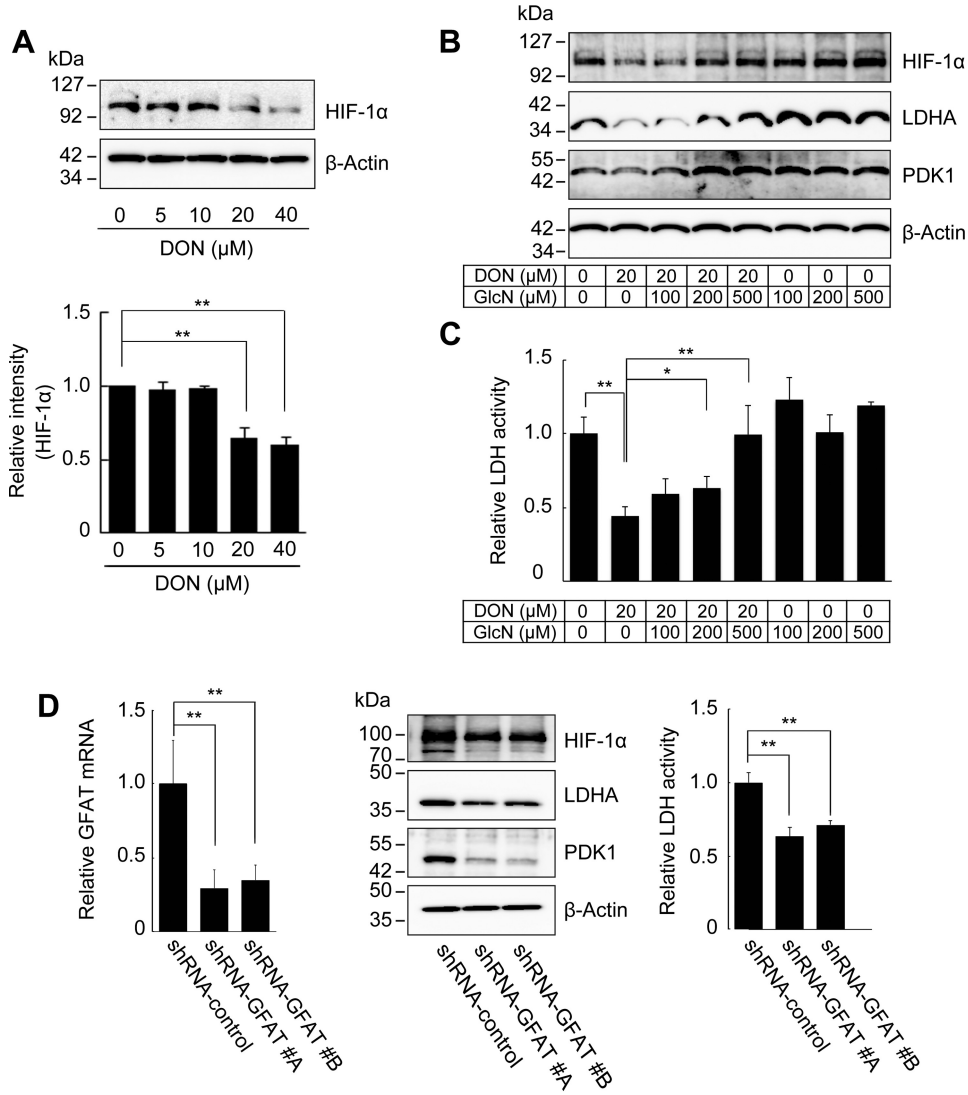

FIGURE 7. **HBP-dependent regulation of HIF-1α expression and glycolysis.** *A*, Western blot analysis for the expression of HIF-1α after inhibition of the HBP. Has2$^{\Delta Neo}$ cells were treated with various concentrations of the GFAT1 antagonist DON for 72 h. Western blot analysis was conducted to determine the expression of HIF-1α. β-Actin was used as an internal control. Band intensities were quantified by densitometric analysis using ImageJ software. Data represent the mean ± S.D. (*error bars*) of three independent experiments. **, $p < 0.01$ as compared with untreated control cells. *B*, Western blot analysis for the expression of HIF-1α, LDHA, and PDK1 in Has2$^{\Delta Neo}$ cells treated with DON in the absence or presence of various concentrations of GlcN. *C*, analysis of LDH activity in Has2$^{\Delta Neo}$ cells treated with DON in the absence or presence of various concentrations of GlcN. Data represent the mean ± S.D. of three independent experiments. *, $p < 0.05$; **, $p < 0.01$ as compared with untreated control cells. *D*, effects of GFAT1 silencing on glycolytic program in Has2-overexpressing cells. Has2$^{\Delta Neo}$ cells were infected with lentiviruses carrying two different inhibitory shRNAs (#*A* and #*B*) targeting GFAT1 or control shRNA. The introduced cells were then analyzed for GFAT1 mRNA expression by qRT-PCR. The expression of HIF-1α, LDHA, and PDK1 in the GFAT1 knockdown cells was also evaluated by Western blotting analysis. Cell lysates from the GFAT1 knockdown cells were measured for LDH activity. Data represent the mean ± S.D. of three independent experiments. **, $p < 0.01$ as compared with the control shRNA cells.

CD44v3 to propagate the stemness of CSCs through complex formation of the stem cell-specific transcription factors Oct4, Sox2, and Nanog (32). Among CD44 variant isoforms, CD44v6 has also been demonstrated to promote the growth of CSCs partially through an Akt-mediated pathway and confer metastatic potential (33, 34). In addition to such critical roles of CD44 in maintaining and propagating CSCs, our previous investigation partly suggested an involvement of a CD44-independent pathway in the control of HA-induced CSC propagation (12). The present results further support the idea that HA plays a key role in regulating the energy metabolism of CSCs through a biosynthetic process instead of as a microenvironmental cue.

An earlier study demonstrated that an intracellular domain (CD44-ICD) generated by the cleavage of intact CD44 could induce the expression of HIF-1α-responsive genes irrespective of HIF-1α (35). Because CD44-positive CSCs are known to preferentially adopt aerobic glycolysis for survival (36), it is reasonable to speculate that CD44 is not only a CSC marker but also a mediator for maintaining the metabolic features of CSCs by up-regulating the transcription of prominent regulatory enzymes in oxidative glycolysis. However, the reported findings that CD44-ICD suppressed HIF-1α expression in either normoxic or hypoxic conditions are inconsistent with the fact that HIF-1α is highly expressed in HA-overproducing cancer cells. It is

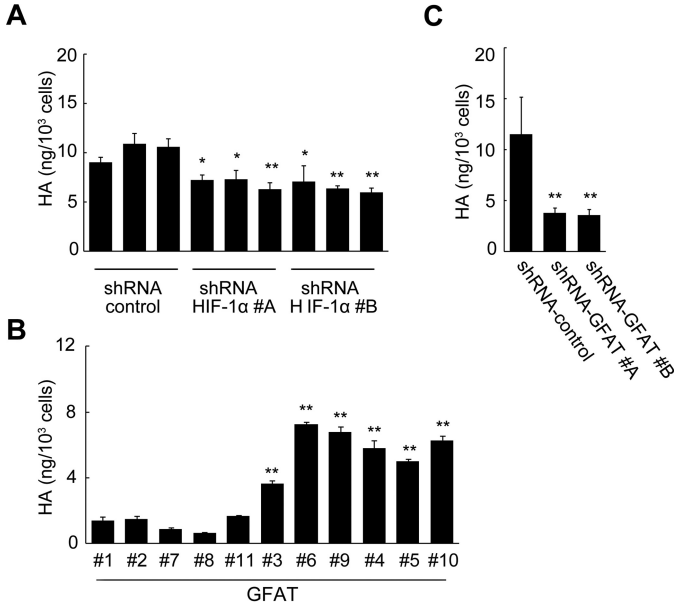

FIGURE 8. **Feedback regulation of HA production by HBP-coupled HIF-1 signaling.** *A*, effects of HIF-1α knockdown on HA production. Has2$^{\Delta Neo}$ cells carrying two different HIF-1α shRNAs (#*A* and #*B*) or a control shRNA were measured for HA content in the conditioned medium. *B* and *C*, effects of GFAT1 overexpression or knockdown on HA production. *B*, Has2^{+Neo} cells expressing various levels of GFAT1 were measured for HA content in the conditioned medium. *C*, Has2$^{\Delta Neo}$ cells carrying two different GFAT1 shRNAs (#*A* and #*B*) or a control shRNA were measured for HA content in the conditioned medium. Data represent the mean ± S.D. (*error bars*) of three independent experiments. *, $p < 0.05$; **, $p < 0.01$ as compared with control shRNA cells.

therefore unlikely that HA-CD44 interactions stimulate the transcription of glycolytic enzymes through the generation of CD44-ICD in HA-overproducing cells.

In conclusion, the present study highlights a novel function of HA in the regulation of energy metabolism via a biosynthetic mechanism to provide a better understanding of the metabolic networks governing cancer cell stemness. Our findings may contribute to the design of new therapeutic strategies through metabolic intervention in CSCs.

Experimental Procedures

Transgenic and Knock-out Mouse Lines—Has2 conditional transgenic (cTg) mice were generated as described previously (37) and cross-bred with mouse mammary tumor virus-Neu (MMTV-Neu) mammary tumor model mice (Charles River Laboratories International, Inc., Wilmington, MA) to generate Has2^{+Neo} mice. MMTV-Neu mice were cross-bred with B6129-TgN (MMTV-cre)4Mam (MMTV-Cre) mice (Jackson Laboratory, Bar Harbor, ME) expressing Cre recombinase under the control of the MMTV promoter to generate MMTV-Neu/MMTV-Cre double transgenic mice. The Has2^{+Neo} mice were further crossed with MMTV-Neu/MMTV-Cre double transgenic mice to generate Has2$^{\Delta Neo}$ mice (Fig. 1*A*).

Has2 conditional knock-out (Has2$^{flox/flox}$) mice were generated as described previously (38) and back-crossed for 12 generations to FVB/N-Tg(MMTV-PyVT)634Mul/J mice (Jackson Laboratory) to generate mammary tumor model mice (Fig. 1*C*). Animal care and all experimental procedures using animal models were performed in accordance with established guidelines and were approved by the Kyoto Sangyo University ethics committee for animal care, handling, and termination.

Establishment of Primary Breast Carcinoma Cells—Has2-overexpressing Has2$^{\Delta Neo}$ and control Has2^{+Neo} breast cancer cells were established as described previously (37, 39). Has2$^{flox/flox}$ breast carcinoma cells were established from primary mammary tumors that had developed spontaneously in Has2$^{flox/flox}$ tumor model mice harboring homozygous Has2 floxed alleles by the method described previously (Fig. 1*C*) (39).

Establishment of Has2-overexpressing and -deficient Breast Carcinoma Cells—Stable cell lines constitutively expressing the Has2 transgene were established from Neu tumor cells that were derived from primary mammary tumors developed in the MMTV-Neu mammary tumor model mice as described previously (12). Has2 #3 and #4 transfectants exhibiting moderate and high levels of HA production, respectively, were chosen for further experiments (Fig. 1, *B* and *D*). Mock transfectants were also established as a negative control. A side population of Has2^{+Neo} cells was infected with a retrovirus carrying the tamoxifen-dependent Cre recombinase (CreER^{T2}), and then stable Cre #2 and Cre #7 clones were selected as described previously (12). To generate Has2-overexpressing Cre #2 (+4-OHT) and Cre #7 (+4-OHT) cells, the neomycin-resistant gene (Neo) cassette of the *Has2* transgene was deleted by CreER^{T2}-mediated recombination in response to 4-OHT as described previously (Fig. 1*B*) (12). Has2$^{flox/flox}$ breast carcinoma cells were infected with the AxCANCre adenovirus carrying the Cre recombinase gene driven by a CAG promoter to generate Has2-deficient Has2$^{\Delta/\Delta}$ cells (Fig. 1*C*). Has2$^{flox/flox}$ cells infected with the AxCANLacZ adenovirus carrying the β-galactosidase (*LacZ*) gene served as a control (Has2$^{flox/flox}$ cells). Has2-overexpressing and -deficient breast carcinoma cells are illustrated schematically in Fig. 1, and their characteristics are summarized in Table 1.

Cell Culture Conditions—All cells were grown either at normoxia in an air-jacketed CO_2 incubator (5% CO_2) or at hypoxia (1% O_2, 5% CO_2) in a multigas incubator (Wakenbtech, Osaka, Japan) in which N_2 gas displaced O_2.

HA Measurement—HA concentrations were determined by a competitive ELISA-like assay, as described previously (37).

Metabolomic Analysis—Breast carcinoma cells (1×10^6 cells/sample) were used for the extraction of intracellular metabolites. Culture medium was aspirated from dishes, and cells were washed twice with a 5% mannitol solution. The cells were then treated with 800 μl of methanol and left at rest for 30 s to inactivate enzymes. Next, cell extracts were treated with 550 μl of Milli-Q water containing internal standards (H3304-1002, Human Metabolome Technologies, Inc., Tsuruoka, Yamagata, Japan) and left at rest for another 30 s. The obtained extracts were centrifuged at 2,300 × *g* and 4 °C for 5 min, and then 800 μl of the upper aqueous layer was centrifugally filtered through a Millipore 5 kDa cut-off filter (Millipore, Billerica, MA) at 9,100 × *g* and 4 °C for 120 min to remove proteins. Last, the filtrates were centrifugally concentrated and resuspended in 50 μl of Milli-Q water for CE-TOF/MS analysis. Metabolomic measurements were carried out externally by Human Metabolome Technology, Inc.

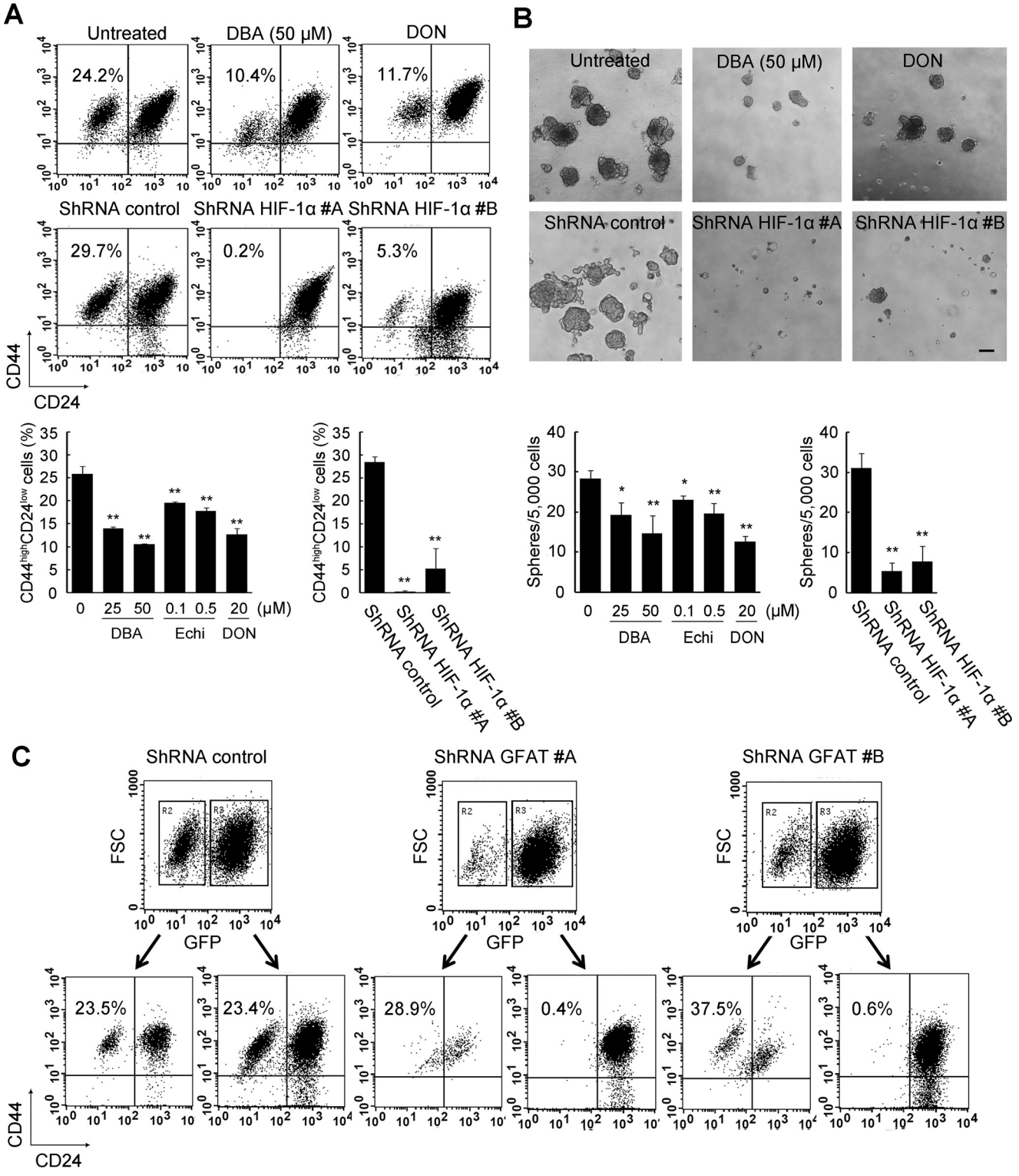

FIGURE 9. **Significance of HBP and HIF-1 signaling in CSC-like properties.** *A*, flow cytometric analysis of the $CD44^{high}/CD24^{low}$ subpopulation after pharmacological inhibition or gene silencing of HIF-1α. $Has2^{\Delta Neo}$ cells were treated with HIF-1α inhibitors (25 or 50 μM DBA and 0.1 or 0.5 μM echinomycin (*Echi*)) for 7 days. $Has2^{\Delta Neo}$ cells were also treated with a GFAT inhibitor (20 μM DON) for 7 days. Treated cells were analyzed for CD24 and CD44 expression by flow cytometry. HIF-1α knockdown cells were also subjected to flow cytometric analysis. Data represent the mean ± S.D. (*error bars*) of three independent experiments. **, $p < 0.01$ as compared with untreated or control cells. *B*, mammosphere formation after pharmacological inhibition or gene silencing. $Has2^{\Delta Neo}$ cells treated with an HIF-1α or GFAT inhibitor were examined for mammosphere formation. HIF-1α knockdown cells were also examined for mammosphere formation. Representative images of mammospheres were taken, and mammosphere number was counted under a phase-contrast microscope. *Scale bar*, 100 μm. Data represent the mean ± S.D. of three independent experiments. *, $p < 0.05$; **, $p < 0.01$. *C*, flow cytometric analysis of the $CD44^{high}/CD24^{low}$ subpopulation after gene silencing of GFAT1. Two different shRNAs (*#A* and *#B*) against murine GFAT1 mRNA were introduced into $Has2^{\Delta Neo}$ cells using a lentiviral vector. The introduced cells were analyzed for GFP expression. Both GFP-positive and -negative cells were further analyzed for CD24 and CD44 expression by flow cytometry.

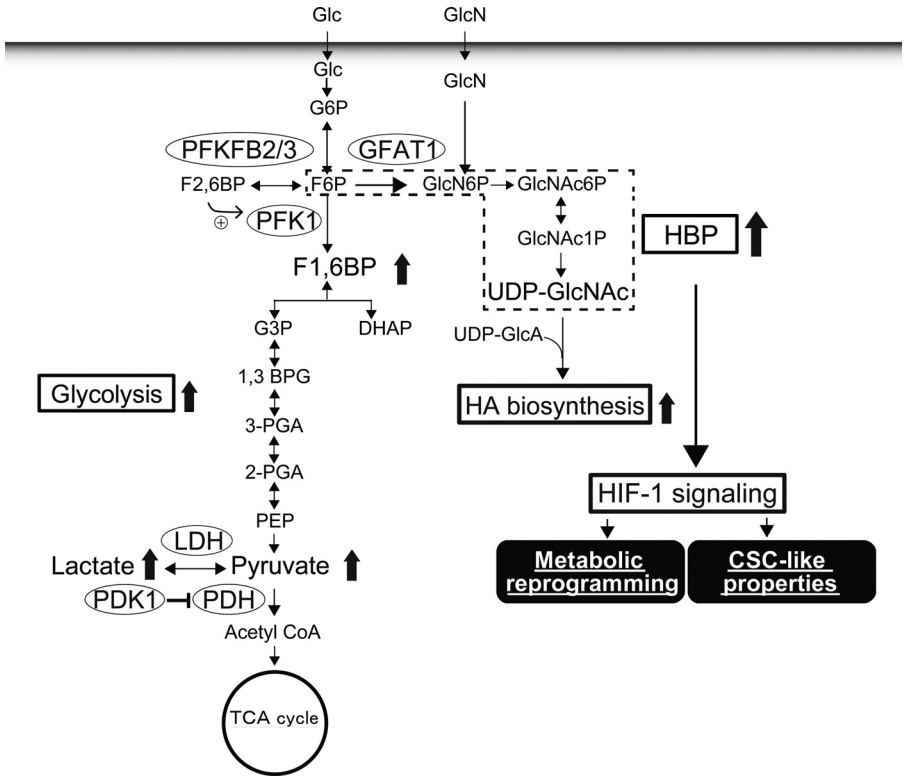

FIGURE 10. **A proposed model for metabolic reprogramming driven by HA overproduction.** Elevated HA biosynthesis evokes HIF-1α signaling through acceleration of HBP flux. The HIF-1α signaling may constitute a feed-forward signaling mechanism required for metabolic reprogramming toward glycolysis and the expression of CSC-like properties. *1,3 BPG*, 1,3-bisphosphoglycerate; *2-PGA*, 2-phosphoglycerate; *GlcNAc6P*, *N*-acetylglucosamine 6-phosphate; *GlcNAc1P*; *N*-acetylglucosamine 1-phosphate; TCA, tricarboxylic acid.

CE-TOF/MS Analysis—CE-TOF/MS was carried out using an Agilent CE capillary electrophoresis system equipped with an Agilent 6210 time-of-flight mass spectrometer, Agilent 1100 isocratic HPLC pump, Agilent G1603A CE-MS adapter kit, and Agilent G1607A CE-ESI-MS sprayer kit (Agilent Technologies, Waldbronn, Germany). The systems were controlled by Agilent G2201AA ChemStation software version B.03.01 for CE (Agilent Technologies). The metabolites were analyzed using a fused silica capillary (50-μm inner diameter $\times$ 80-cm total length) with commercial electrophoresis buffer (Solution ID: H3301-1001 for cation analysis and H3302-1021 for anion analysis, Human Metabolome Technologies Inc.) as the electrolyte. Samples were injected at a pressure of 50 millibars for 10 s ($\sim$10 nl) for cation analysis and 25 s ($\sim$25 nl) for anion analysis. The ions were scanned from *m*/*z* 50 to 1,000. Other conditions were set as described previously (40–42).

Peaks were extracted using MasterHands automatic integration software (Keio University, Tsuruoka, Yamagata, Japan) to obtain *m/z* values, migration time for CE-TOF/MS measurement (MT), and peak area (43). Signal peaks corresponding to isotopomers, adduct ions, and other ion products of known metabolites were excluded; the remaining peaks were annotated with putative metabolites from the HMT metabolite database based on their MT; and then *m/z* values were determined by TOF/MS. The tolerance range for peak annotation was configured at $\pm$0.5 min for MT and $\pm$10 ppm for *m/z*. Peak areas were normalized using those of internal standards, and the metabolites were quantified by comparing their peak areas against calibration curves generated using internal standardization techniques. The measured metabolite concentrations were normalized using cell numbers to obtain the amount of metabolite contained per 10^6 cells of each sample.

Ion Pair Reversed-phase LC-ESI-MS for Isotopomer Analysis of Nucleotide Sugars—For the preparation of ^{13}C-labeled nucleotide sugars, breast carcinoma cells were seeded into 35-mm dishes (1×10^5 cells/dish) and cultured at 37 °C and 5% CO_2 for 24 h in glucose-free DMEM supplemented with 5.5 mM natural glucose and then further cultured in glucose-free DMEM supplemented with 5.5 mM [$^{13}C_6$]glucose (Sigma) for up to 6 h. Nucleotide sugars were prepared and analyzed according to the method reported previously (44). Ion pair reversed-phase LC-ESI-MS was performed using an Agilent 1100 series HPLC system (Agilent Technologies) coupled to an Esquire HCT ion trap mass spectrometer (Bruker Daltonics, Bremen, Germany) as described previously (13). The replacement ratios were calculated as possible combinations of labeled and natural isotopic ions, as described previously (13).

Inhibitor Treatments—Has2$^{\Delta Neo}$ cells were seeded into 6-well plates (2×10^5 cells/well) and cultured at 37 °C and 5% CO_2 for 24 h in DMEM containing 10% FBS. The cells were treated with 20 μM DON (Sigma) in the presence or absence of 0.1–0.5 mM D-glucosamine hydrochloride (Wako Pure Chemical Industries, Osaka, Japan) for 3 days. Has2$^{\Delta Neo}$ cells were treated with 0–50 nM echinomycin (Sigma) in serum-free DMEM for 3 days. Whole cell lysates were analyzed for LDH activity, and the expression of glycolytic enzymes was assessed by Western blot analysis. Culture medium from the treated cells was collected and measured for lactate production. Has2$^{\Delta Neo}$ cells were treated with 0–50 μM

DBA (Abcam, Cambridge, MA), 0–0.5 μM echinomycin, or 20 μM DON for 7 days before analysis of CD24 and CD44 expression by flow cytometry.

SDS-PAGE and Western Blotting—Breast carcinoma cells were lysed in radioimmune precipitation assay buffer (25 mM Tris-HCl, pH 7.6, 150 mM NaCl, 1% Nonidet P-40, 1% sodium deoxycholate, and 0.1% SDS) containing a protease and phosphatase inhibitor mixture (Nacalai Tesque, Osaka, Japan). Protein contents were determined with a Pierce Microplate BCA protein assay kit (Thermo Scientific, Rockford, IL) according to the manufacturer's instructions. Equal amounts of protein samples (2 μg) were then subjected to SDS-PAGE on 8–12% polyacrylamide gels. After protein transfer to PVDF membranes (Millipore), the membranes were blocked with 5% skim milk in TBST (50 mM Tris-HCl, pH 7.4, 138 mM NaCl, 2.7 mM KCl, and 0.1% Tween 20) at room temperature for 60 min and then incubated with primary antibodies against HIF-1α (1:1,000 dilution; Novus Biologicals, Littleton, CO), GFAT1, ALDOA, enolase-1, enolase-2, PDK1, PFKFB2, PFKFB3, PGAM1, or LDHA (1:1,000 dilution; Cell Signaling Technology, Danvers, MA) at 4 °C overnight. The membranes were subsequently washed with TBST and incubated with horseradish peroxidase-conjugated secondary antibodies (1:1,000 dilution; Cell Signaling Technology) for 60 min before visualization with Western blotting detection reagents (Wako Pure Chemical Industries). Detection of chemiluminescent signals was performed on an ImageQuant LAS4000 Mini Luminescent image analyzer (GE Healthcare). Band intensities were quantified by densitometric analysis using ImageJ software (National Institutes of Health, Bethesda, MD).

qRT-PCR—Total RNA from breast carcinoma cells was isolated using the Qiagen RNeasy Mini kit (Qiagen, Germantown, MD). Glycolytic pathway-focused gene expression analysis was performed using the glucose metabolism RT^2 Profiler PCR array system according to the manufacturer's instructions (Qiagen). Data were analyzed using the RT^2 Profiler program (Qiagen) and normalized to five housekeeping genes: β_2-microglobulin, GAPDH, β-glucuronidase, β-actin, and heat shock protein 90 kDa α (cytosolic) class B member 1.

cDNA was synthesized with the PrimeScript RT Reagent kit (Takara Bio, Shiga, Japan) according to the manufacturer's instructions. TaqMan gene expression assays (Applied Biosystems, Foster City, CA) were used for the gene expression analyses of murine HIF-1α (Mm00468869_m1) and murine GFAT1 (Mm01183874_m1). The qRT-PCR condition for gene expression was one cycle at 95 °C for 30 s followed by 40 cycles at 95 °C for 3 s and 60 °C for 25 s. For the murine *Has2* gene, qRT-PCR was performed as described previously (37). Relative mRNA expression was normalized using GAPDH expression.

Measurement of Lactate Production—Breast carcinoma cells were seeded into 96-well plates at 1×10^4 cells/well and cultured at 37 °C and 5% CO_2 for 24 h in DMEM containing 10% FBS. The culture medium was then changed to serum-free DMEM, and the cells were cultured for an additional 24 h. Lactate concentration in the conditioned medium was measured using the lactate assay kit (BioVision, Milpitas, CA) according to the manufacturer's instructions and calculated as the amount of lactate normalized to cell numbers.

Measurement of LDH Activity—Breast carcinoma cells were seeded in 100-mm dishes (1×10^6 cells/dish) and cultured at 37 °C and 5% CO_2 for 2 days in DMEM containing 10% FBS. The cells were harvested and homogenized in 0.5 ml of cold assay buffer. Supernatants were collected after centrifugation at $10,000 \times g$ for 15 min at 4 °C, and intracellular LDH activity was determined using an LDH activity assay kit (BioVision) according to the manufacturer's instructions. LDH activity was normalized to protein amounts.

Construction of GFAT1 Expression Plasmids and Isolation of Stable Transfectants—Human GFAT1 full-length cDNA in a pCMV6-XL5 cloning vector (OriGene Technologies, Inc., Rockville, MD) was subcloned into a pIREShyg mammalian expression vector (Clontech, Mountain View, CA) using the Gibson assembly method (New England Biolabs, Inc., Ipswich, MA). The construct was transfected into $Has2^{+Neo}$ breast cancer cells using FuGENE 6 transfection reagent (Promega, Madison, WI) according to the manufacturer's instructions. Stable transfectants were selected in the presence of 200 μg/ml hygromycin B (Nacalai Tesque).

Viral Preparation and Transduction—Recombinant lentivirus particles were produced by co-transfecting the Lenti-X 293T cell line (Takara Bio) with the pGFP-C-shLenti (OriGene) lentiviral vector carrying the shRNA of murine GFAT1 (Gene ID 14583) together with packaging constructs (Lenti-vpak lentiviral packaging kit, OriGene) according to the manufacturer's instructions. Control lentiviruses composed of non-targeting shRNA (OriGene) were used as a negative control. For viral infection, $Has2^{\Delta Neo}$ cells were infected with lentiviruses using the RetroNectin-bound virus infection method according to the manufacturer's instructions (Takara Bio). Introduced cells were selected in the presence of 10 μg/ml puromycin dihydrochloride for 12 h and further maintained in 5 μg/ml puromycin dihydrochloride for 7 days. Recombinant retrovirus particles were produced by co-transfecting a highly transfectable GP2-293 cell line with the pRFP-C-RS (OriGene) retroviral vector carrying the shRNA of murine HIF-1α together with packaging constructs (Retroviral Packaging Systems, Takara Bio) according to the manufacturer's instructions. $Has2^{\Delta Neo}$ cells were exposed to retroviruses for 8 h and further cultured for 2 days. Stable clones were selected in the presence of 2.5 μg/ml puromycin dihydrochloride.

Flow Cytometric Analysis—Breast cancer cells were suspended in cold PBS supplemented with 1% FBS, and 50 μl of cell suspension (1×10^7 cells/ml) were incubated with phycoerythrin-conjugated anti-CD44 (1:160 dilution; eBioscience, San Diego, CA) and FITC-conjugated anti-CD24 antibodies (1:50 dilution; eBioscience) for 60 min at 4 °C. For GFP-positive cells, phycoerythrin/Cy5-conjugated anti-CD24 antibody (1:50 dilution; eBioscience) was used as a first antibody. The cells were washed, resuspended in cold PBS supplemented with 1% FBS, and then filtered through cell strainers. A total of 10,000 viable cells were analyzed with a FACSCalibur device (BD Biosciences) and CellQuest software version 5.1.

Mammosphere Formation Assay—The mammosphere formation assay was performed as described previously (12, 45).

Statistical Analysis—The Wilcoxon matched pairs test was adopted to statistically compare metabolite levels between each group. The two-tailed Student's *t* test was employed for other

statistical analyses. Results are reported as mean ± S.D. values. A p value of <0.05 was considered to be statistically significant.

Author Contributions—T. C. and N. I. designed research. P. K. and N. T. helped to conduct the experiment. T. C., P. O., T. I., M. H., N. M., C. C., M. K., K. N., I. K., N. T., and N. I. performed research. T. C., P. O., T. I., M. H., N. M., K. N., I. K., and N. I. analyzed data. T. C., P. O., K. N., I. K., and N. I. wrote the manuscript. All authors reviewed the manuscript.

Acknowledgments—We thank Dr. Izumu Saito (Tokyo University) for providing the AxCANCre adenovirus, Dr. Tyler Jacks (Massachusetts Institute of Technology) for the MSCV CreER^{T2} puro, and Dr. Jun-ichi Miyazaki (Osaka University) for the CAG promoter.

References

1. Warburg, O. (1956) On the origin of cancer cells. *Science* **123,** 309–314
2. Vander Heiden, M. G., Cantley, L. C., and Thompson, C. B. (2009) Understanding the Warburg effect: the metabolic requirements of cell proliferation. *Science* **324,** 1029–1033
3. Menendez, J. A., Joven, J., Cufí, S., Corominas-Faja, B., Oliveras-Ferraros, C., Cuyàs, E., Martin-Castillo, B., López-Bonet, E., Alarcón, T., and Vazquez-Martin, A. (2013) The Warburg effect version 2.0: metabolic reprogramming of cancer stem cells. *Cell Cycle* **12,** 1166–1179
4. Ito, K., and Suda, T. (2014) Metabolic requirements for the maintenance of self-renewing stem cells. *Nat. Rev. Mol. Cell Biol.* **15,** 243–256
5. Semenza, G. L. (2003) Targeting HIF-1 for cancer therapy. *Nat. Rev. Cancer* **3,** 721–732
6. Huang, L. E., Gu, J., Schau, M., and Bunn, H. F. (1998) Regulation of hypoxia-inducible factor 1α is mediated by an O_2-dependent degradation domain via the ubiquitin-proteasome pathway. *Proc. Natl. Acad. Sci. U.S.A.* **95,** 7987–7992
7. Agani, F., and Jiang, B. H. (2013) Oxygen-independent regulation of HIF-1: novel involvement of PI3K/AKT/mTOR pathway in cancer. *Curr. Cancer Drug Targets* **13,** 245–251
8. Semenza, G. L. (2002) HIF-1 and tumor progression: pathophysiology and therapeutics. *Trends Mol. Med.* **8,** S62–S67
9. Ferrer, C. M., Lynch, T. P., Sodi, V. L., Falcone, J. N., Schwab, L. P., Peacock, D. L., Vocadlo, D. J., Seagroves, T. N., and Reginato, M. J. (2014) *O*-GlcNAcylation regulates cancer metabolism and survival stress signaling via regulation of the HIF-1 pathway. *Mol. Cell* **54,** 820–831
10. Itkonen, H. M., Minner, S., Guldvik, I. J., Sandmann, M. J., Tsourlakis, M. C., Berge, V., Svindland, A., Schlomm, T., and Mills, I. G. (2013) *O*-GlcNAc transferase integrates metabolic pathways to regulate the stability of c-MYC in human prostate cancer cells. *Cancer Res.* **73,** 5277–5287
11. Toole, B. P. (2004) Hyaluronan: from extracellular glue to pericellular cue. *Nat. Rev. Cancer* **4,** 528–539
12. Chanmee, T., Ontong, P., Mochizuki, N., Kongtawelert, P., Konno, K., and Itano, N. (2014) Excessive hyaluronan production promotes acquisition of cancer stem cell signatures through the coordinated regulation of Twist and the transforming growth factor β (TGF-β)-Snail signaling axis. *J. Biol. Chem.* **289,** 26038–26056
13. Nakajima, K., Ito, E., Ohtsubo, K., Shirato, K., Takamiya, R., Kitazume, S., Angata, T., and Taniguchi, N. (2013) Mass isotopomer analysis of metabolically labeled nucleotide sugars and *N*- and *O*-glycans for tracing nucleotide sugar metabolisms. *Mol. Cell Proteomics* **12,** 2468–2480
14. Semenza, G. L., Roth, P. H., Fang, H. M., and Wang, G. L. (1994) Transcriptional regulation of genes encoding glycolytic enzymes by hypoxia-inducible factor 1. *J. Biol. Chem.* **269,** 23757–23763
15. Denko, N. C. (2008) Hypoxia, HIF1 and glucose metabolism in the solid tumour. *Nat. Rev. Cancer* **8,** 705–713
16. Alt, J., Potter, M. C., Rojas, C., and Slusher, B. S. (2015) Bioanalysis of 6-diazo-5-oxo-l-norleucine in plasma and brain by ultra-performance liquid chromatography mass spectrometry. *Anal. Biochem.* **474,** 28–34
17. Hartman, S. C., and McGrath, T. F. (1973) Glutaminase A of *Escherichia coli*: reactions with the substrate analogue, 6-diazo-5-oxonorleucine. *J. Biol. Chem.* **248,** 8506–8510
18. Dontu, G., Abdallah, W. M., Foley, J. M., Jackson, K. W., Clarke, M. F., Kawamura, M. J., and Wicha, M. S. (2003) *In vitro* propagation and transcriptional profiling of human mammary stem/progenitor cells. *Genes Dev.* **17,** 1253–1270
19. Kohn, A. D., Summers, S. A., Birnbaum, M. J., and Roth, R. A. (1996) Expression of a constitutively active Akt Ser/Thr kinase in 3T3-L1 adipocytes stimulates glucose uptake and glucose transporter 4 translocation. *J. Biol. Chem.* **271,** 31372–31378
20. Morrish, F., Isern, N., Sadilek, M., Jeffrey, M., and Hockenbery, D. M. (2009) c-Myc activates multiple metabolic networks to generate substrates for cell-cycle entry. *Oncogene* **28,** 2485–2491
21. Moon, S. O., Lee, J. H., and Kim, T. J. (1998) Changes in the expression of c-myc, RB and tyrosine-phosphorylated proteins during proliferation of NIH 3T3 cells induced by hyaluronic acid. *Exp. Mol. Med.* **30,** 29–33
22. Vigetti, D., Deleonibus, S., Moretto, P., Karousou, E., Viola, M., Bartolini, B., Hascall, V. C., Tammi, M., De Luca, G., and Passi, A. (2012) Role of UDP-*N*-acetylglucosamine (GlcNAc) and *O*-GlcNAcylation of hyaluronan synthase 2 in the control of chondroitin sulfate and hyaluronan synthesis. *J. Biol. Chem.* **287,** 35544–35555
23. Soeda, A., Park, M., Lee, D., Mintz, A., Androutsellis-Theotokis, A., McKay, R. D., Engh, J., Iwama, T., Kunisada, T., Kassam, A. B., Pollack, I. F., and Park, D. M. (2009) Hypoxia promotes expansion of the CD133-positive glioma stem cells through activation of HIF-1α. *Oncogene* **28,** 3949–3959
24. Treins, C., Giorgetti-Peraldi, S., Murdaca, J., Semenza, G. L., and Van Obberghen, E. (2002) Insulin stimulates hypoxia-inducible factor 1 through a phosphatidylinositol 3-kinase/target of rapamycin-dependent signaling pathway. *J. Biol. Chem.* **277,** 27975–27981
25. Jung, Y. J., Isaacs, J. S., Lee, S., Trepel, J., and Neckers, L. (2003) IL-1β-mediated up-regulation of HIF-1α via an NFκB/COX-2 pathway identifies HIF-1 as a critical link between inflammation and oncogenesis. *FASEB J.* **17,** 2115–2117
26. Zhou, J., Schmid, T., and Brüne, B. (2003) Tumor necrosis factor-α causes accumulation of a ubiquitinated form of hypoxia inducible factor-1α through a nuclear factor-κB-dependent pathway. *Mol. Biol. Cell* **14,** 2216–2225
27. Thomas, G. V., Tran, C., Mellinghoff, I. K., Welsbie, D. S., Chan, E., Fueger, B., Czernin, J., and Sawyers, C. L. (2006) Hypoxia-inducible factor determines sensitivity to inhibitors of mTOR in kidney cancer. *Nat. Med.* **12,** 122–127
28. Zundel, W., Schindler, C., Haas-Kogan, D., Koong, A., Kaper, F., Chen, E., Gottschalk, A. R., Ryan, H. E., Johnson, R. S., Jefferson, A. B., Stokoe, D., and Giaccia, A. J. (2000) Loss of PTEN facilitates HIF-1-mediated gene expression. *Genes Dev.* **14,** 391–396
29. Mahon, P. C., Hirota, K., and Semenza, G. L. (2001) FIH-1: a novel protein that interacts with HIF-1alpha and VHL to mediate repression of HIF-1 transcriptional activity. *Genes Dev.* **15,** 2675–2686
30. Patten, D. A., Lafleur, V. N., Robitaille, G. A., Chan, D. A., Giaccia, A. J., and Richard, D. E. (2010) Hypoxia-inducible factor-1 activation in nonhypoxic conditions: the essential role of mitochondrial-derived reactive oxygen species. *Mol. Biol. Cell* **21,** 3247–3257
31. Calvani, M., Comito, G., Giannoni, E., and Chiarugi, P. (2012) Time-dependent stabilization of hypoxia inducible factor-1α by different intracellular sources of reactive oxygen species. *PLoS One* **7,** e38388
32. Bourguignon, L. Y., Wong, G., Earle, C., and Chen, L. (2012) Hyaluronan-CD44v3 interaction with Oct4-Sox2-Nanog promotes miR-302 expression leading to self-renewal, clonal formation, and cisplatin resistance in cancer stem cells from head and neck squamous cell carcinoma. *J. Biol. Chem.* **287,** 32800–32824
33. Jijiwa, M., Demir, H., Gupta, S., Leung, C., Joshi, K., Orozco, N., Huang, T., Yildiz, V. O., Shibahara, I., de Jesus, J. A., Yong, W. H., Mischel, P. S., Fernandez, S., Kornblum, H. I., and Nakano, I. (2011) CD44v6 regulates growth of brain tumor stem cells partially through the AKT-mediated pathway. *PLoS One* **6,** e24217

34. Todaro, M., Gaggianesi, M., Catalano, V., Benfante, A., Iovino, F., Biffoni, M., Apuzzo, T., Sperduti, I., Volpe, S., Cocorullo, G., Gulotta, G., Dieli, F., De Maria, R., and Stassi, G. (2014) CD44v6 is a marker of constitutive and reprogrammed cancer stem cells driving colon cancer metastasis. *Cell Stem Cell* **14,** 342–356
35. Miletti-González, K. E., Murphy, K., Kumaran, M. N., Ravindranath, A. K., Wernyj, R. P., Kaur, S., Miles, G. D., Lim, E., Chan, R., Chekmareva, M., Heller, D. S., Foran, D., Chen, W., Reiss, M., Bandera, E. V., *et al.* (2012) Identification of function for CD44 intracytoplasmic domain (CD44-ICD): modulation of matrix metalloproteinase 9 (MMP-9) transcription via novel promoter response element. *J. Biol. Chem.* **287,** 18995–19007
36. Tamada, M., Nagano, O., Tateyama, S., Ohmura, M., Yae, T., Ishimoto, T., Sugihara, E., Onishi, N., Yamamoto, T., Yanagawa, H., Suematsu, M., and Saya, H. (2012) Modulation of glucose metabolism by CD44 contributes to antioxidant status and drug resistance in cancer cells. *Cancer Res.* **72,** 1438–1448
37. Koyama, H., Hibi, T., Isogai, Z., Yoneda, M., Fujimori, M., Amano, J., Kawakubo, M., Kannagi, R., Kimata, K., Taniguchi, S., and Itano, N. (2007) Hyperproduction of hyaluronan in neu-induced mammary tumor accelerates angiogenesis through stromal cell recruitment: possible involvement of versican/PG-M. *Am. J. Pathol.* **170,** 1086–1099
38. Kobayashi, N., Miyoshi, S., Mikami, T., Koyama, H., Kitazawa, M., Takeoka, M., Sano, K., Amano, J., Isogai, Z., Niida, S., Oguri, K., Okayama, M., McDonald, J. A., Kimata, K., Taniguchi, S., and Itano, N. (2010) Hyaluronan deficiency in tumor stroma impairs macrophage trafficking and tumor neovascularization. *Cancer Res.* **70,** 7073–7083
39. Koyama, H., Kobayashi, N., Harada, M., Takeoka, M., Kawai, Y., Sano, K., Fujimori, M., Amano, J., Ohhashi, T., Kannagi, R., Kimata, K., Taniguchi, S., and Itano, N. (2008) Significance of tumor-associated stroma in promotion of intratumoral lymphangiogenesis: pivotal role of a hyaluronan-rich tumor microenvironment. *Am. J. Pathol.* **172,** 179–193
40. Soga, T., and Heiger, D. N. (2000) Amino acid analysis by capillary electrophoresis electrospray ionization mass spectrometry. *Anal. Chem.* **72,** 1236–1241
41. Soga, T., Ueno, Y., Naraoka, H., Ohashi, Y., Tomita, M., and Nishioka, T. (2002) Simultaneous determination of anionic intermediates for *Bacillus subtilis* metabolic pathways by capillary electrophoresis electrospray ionization mass spectrometry. *Anal. Chem.* **74,** 2233–2239
42. Soga, T., Ohashi, Y., Ueno, Y., Naraoka, H., Tomita, M., and Nishioka, T. (2003) Quantitative metabolome analysis using capillary electrophoresis mass spectrometry. *J. Proteome Res.* **2,** 488–494
43. Sugimoto, M., Wong, D. T., Hirayama, A., Soga, T., and Tomita, M. (2010) Capillary electrophoresis mass spectrometry-based saliva metabolomics identified oral, breast and pancreatic cancer-specific profiles. *Metabolomics* **6,** 78–95
44. Nakajima, K., Kitazume, S., Angata, T., Fujinawa, R., Ohtsubo, K., Miyoshi, E., and Taniguchi, N. (2010) Simultaneous determination of nucleotide sugars with ion-pair reversed-phase HPLC. *Glycobiology* **20,** 865–871
45. Klopp, A. H., Lacerda, L., Gupta, A., Debeb, B. G., Solley, T., Li, L., Spaeth, E., Xu, W., Zhang, X., Lewis, M. T., Reuben, J. M., Krishnamurthy, S., Ferrari, M., Gaspar, R., Buchholz, T. A., *et al.* (2010) Mesenchymal stem cells promote mammosphere formation and decrease E-cadherin in normal and malignant breast cells. *PLoS One* **5,** e12180